Calculation of the anomalous exponents in the rapid-change model of passive scalar advection to order ε^3

L. Ts. Adzhemyan, N. V. Antonov, V. A. Barinov, Yu. S. Kabrits, and A. N. Vasil'ev

Department of Theoretical Physics, St. Petersburg University, Uljanovskaja 1, St. Petersburg-Petrodvorez 198504, Russia

The field theoretic renormalization group and operator product expansion are applied to the model of a passive scalar advected by the Gaussian velocity field with zero mean and correlation function $\propto \delta(t - t')/k^{d+\varepsilon}$. Inertial-range anomalous exponents, identified with the critical dimensions of various scalar and tensor composite operators constructed of the scalar gradients, are calculated within the ε expansion to order ε^3 (three-loop approximation), including the exponents in anisotropic sectors. The main goal of the paper is to give the complete derivation of this third-order result, and to present and explain in detail the corresponding calculational techniques. The character and convergence properties of the ε expansion are discussed, the improved ''inverse'' ε expansion is proposed, and the comparison with the existing nonperturbative results is given.

I. INTRODUCTION

The investigation of intermittency and anomalous scaling in fully developed turbulence remains essentially an open theoretical problem. Both the natural and numerical experiments suggest that the deviation from the classical Kolmogorov theory [1] is even more strongly pronounced for a passively advected scalar field than for the velocity field itself; see, e.g., Ref. [2] and literature cited therein. At the same time, the problem of passive advection appears more easily tractable theoretically: even simplified models describing the advection by a ''synthetic'' velocity field with a given Gaussian statistics reproduce many of the anomalous features of genuine turbulent heat or mass transport observed in experiments. Therefore, the problem of passive scalar advection, being of practical importance in itself, may also be viewed as a starting point in studying intermittency and anomalous scaling in the turbulence as a whole. Detailed review of the recent theoretical research on the passive scalar problem and the bibliography can be found in Ref. [3].

Most progress has been achieved for Kraichnan's rapid-change model [4]: for the first time, the anomalous exponents have been derived on the basis of a microscopic model and within controlled approximations [5–8].

In that model, the advection of a passive scalar field $\theta(x) \equiv \theta(t,\mathbf{x})$ is described by the stochastic equation

$$\nabla_t \theta = \nu_0 \partial^2 \theta + f, \quad \nabla_t \equiv \partial_t + v_i \partial_i, \tag{1.1}$$

where $\partial_t \equiv \partial/\partial t$, $\partial_i \equiv \partial/\partial x_i$, ν_0 is the molecular diffusivity coefficient, ∂^2 is the Laplace operator, $\mathbf{v}(x) \equiv \{v_i(x)\}$ is the transverse (owing to the incompressibility) velocity field, and $f \equiv f(x)$ is an artificial Gaussian scalar noise with zero mean and correlation function

$$\langle f(x) f(x') \rangle = \delta(t - t') C(\mathbf{r}/L), \quad \mathbf{r} = \mathbf{x} - \mathbf{x}'. \tag{1.2}$$

The parameter L is an integral scale related to the noise and $C(\mathbf{r}/L)$ is some function finite as $L \to \infty$.

In the real problem, the field $\mathbf{v}(x)$ satisfies the Navier-Stokes equation. In the rapid-change model it obeys a Gaussian distribution with zero mean and correlation function

$$\langle v_i(x) v_j(x') \rangle = D_0 \delta(t - t')(2\pi)^{-d} \int d\mathbf{k} P_{ij}(\mathbf{k}) N_k$$

$$\times \exp[i\mathbf{k} \cdot (\mathbf{x} - \mathbf{x}')],$$

$$N_k = \Theta(k - m)k^{-d-\varepsilon}, \tag{1.3}$$

where $P_{ij}(\mathbf{k}) = \delta_{ij} - k_i k_j/k^2$ is the transverse projector, $k \equiv |\mathbf{k}|$, $D_0 > 0$ is an amplitude factor, d is the dimensionality of the $\mathbf{x}$ space, $\Theta(\cdots)$ is the step function, and $0 < \varepsilon < 2$ is a parameter with the real (''Kolmogorov'') value $\varepsilon = 4/3$.

The infrared (IR) regularization is provided by the cutoff in the integral (1.3) from below at $k = m$, where $m \equiv 1/l$ is the reciprocal of another integral scale l. The anomalous exponents are independent of the precise form of the IR regularization; the sharp cutoff is the most convenient choice from the calculational viewpoints. In what follows, we shall not distinguish the two IR scales, setting $L \sim l$. The relations

$$D_0/\nu_0 = g_0 = \Lambda^\varepsilon \tag{1.4}$$

define the coupling constant g_0 (i.e., the formal expansion parameter in the ordinary perturbation theory) and the characteristic ultraviolet (UV) momentum scale Λ.

The issue of interest is, in particular, the behavior of the equal-time structure functions

$$S_n(\mathbf{r}) = \langle [\theta(t,\mathbf{x}) - \theta(t,\mathbf{x}')]^n \rangle \tag{1.5}$$

in the inertial-convective range $\Lambda \gg 1/r \gg m$.

In the isotropic model (1.1)–(1.3), the odd multipoint correlation functions of the scalar field vanish, while the even equal-time functions satisfy linear partial differential equations [4–6]. The solution for the pair correlation function is obtained explicitly; it shows that the structure function $S_2 \propto r^{2-\varepsilon}$ is finite at $m = 0$ [4]. The higher-order correlators are not found explicitly, but their inertial-range behavior can be

extracted from the analysis of the nontrivial zero modes of the corresponding differential operators in the limits $\varepsilon \to 0$ [5,7], $1/d \to 0$ [6], or $\varepsilon \to 2$ [7,8]. It was shown that the even structure functions in the inertial-convective range exhibit anomalous scaling behavior,

$$S_n(r) \propto D_0^{-n/2} r^{n(1-\varepsilon/2)} (mr)^{\Delta_n}, \quad r = |\mathbf{x} - \mathbf{x}'| \quad (1.6)$$

with negative anomalous exponents Δ_n, whose first terms of the expansion in ε [5] and $1/d$ [6] have the forms

$$\Delta_n = -n(n-2)\varepsilon/2(d+2) + O(\varepsilon^2) = -n(n-2)\varepsilon/2d$$
$$+ O(1/d^2). \quad (1.7)$$

Another quantity of interest is the local dissipation rate of scalar fluctuations, $E(x) = \nu_0 \partial_i \theta(x) \partial_i \theta(x)$. The equal-time correlation functions of its powers in the inertial range have the forms [5,6],

$$\langle E^n(x) E^p(x') \rangle \propto (\Lambda r)^{-\Delta_{2n}-\Delta_{2p}} (mr)^{\Delta_{2n+2p}} \quad (1.8)$$

with Λ from Eq. (1.4) and Δ_n from Eq. (1.6). Relations of the form (1.8) are characteristic of the models with multifractal behavior [9].

In Ref. [10] and subsequent papers [11–15], the field theoretic renormalization group (RG) and operator product expansion (OPE) were applied to model (1.1)–(1.3). In the RG approach, the anomalous scaling for the structure functions and various pair correlators is established as a consequence of the existence of ''dargerous'' composite operators in the corresponding operator product expansions whose *negative* critical dimensions are identified with the anomalous exponents Δ_n. This allows one to construct a systematic perturbation expansion for the anomalous exponents, analogous to the well-known ε expansion in the RG theory of critical behavior.

The key role in the RG and OPE approach to model (1.1)–(1.3) is played by the critical dimensions Δ_{nl}, associated with the irreducible tensor composite operators

$$F_{nl} = \mathcal{P}_{\text{ir}}[\partial_{i_1}\theta \cdots \partial_{i_l}\theta(\partial_i\theta \partial_i\theta)^p], \quad (1.9)$$

where l is the number of the free vector indices and $n = l + 2p$ is the total number of the fields θ entering into the operator; the vector indices of the symbol F_{nl} are omitted. The symbol $\mathcal{P}_{\text{ir}}$ denotes the irreducible part, obtained by subtracting the appropriate expression involving the delta symbols, such that the resulting tensor is traceless with respect to any pair of indices. In particular, $\mathcal{P}_{\text{ir}}[\partial_i\theta \partial_j\theta] = \partial_i\theta \partial_j\theta - \delta_{ij}(\partial_k\theta \partial_k\theta)/d$ and so on.

The dimension $\Delta_n \equiv \Delta_{n0}$ of the scalar operator is nothing other than the anomalous exponent in Eq. (1.6); see Ref. [10]. The dimensions with $l \neq 0$ come into play if the forcing (1.2) becomes anisotropic: Δ_{nl} corresponds to the leading zero-mode contribution to the lth term of the Legendre decomposition for the function S_n; see Ref. [13]. They can be systematically calculated as a series in ε,

$$\Delta_{nl} = \sum_{k=1}^{\infty} \Delta_{nl}^{(k)} \varepsilon^k \quad (1.10)$$

with the first-order coefficient [13]

$$\Delta_{nl}^{(1)} = -\frac{n(n-2)}{2(d+2)} + \frac{(d+1)l(d+l-2)}{2(d-1)(d+2)}. \quad (1.11)$$

For $l=0$ this gives the result of [5], while for $n=3$ and $l=1,3$ the results of Refs. [7] are recovered. The result (1.11) was rederived later in Refs. [16,17].

The coefficients $\Delta_{n0}^{(2)}$ and $\Delta_{n2}^{(2)}$ were obtained in Ref. [10] for any n and d; the result for general l is presented in [14]. In particular, one has

$$\Delta_{nl}^{(2)} = n(n-2)(0.000\,203n - 0.029\,76) - l^2(0.017\,32n$$
$$+ 0.012\,23) \quad (1.12a)$$

for $d=2$ and

$$\Delta_{nl}^{(2)} = n(n-2)(0.002\,03n - 0.003\,84) - l(l+1)(0.007\,10n$$
$$- 0.006\,19) \quad (1.12b)$$

for $d=3$ (analytical results are too cumbersome and will not be given here; see Refs. [10] for $l=0,2$ and [14] for general l).

The $O(\varepsilon^3)$ contribution to Δ_{nl} was presented in Ref. [15],

$$\Delta_{nl}^{(3)} = n(n-2)(0.004\,54n^2 + 0.064\,86n + 0.065\,05) + l^2$$
$$(-0.019\,74n^2 - 0.104\,23n + 0.240\,94 + 0.017\,48\,l^2) \quad (1.13a)$$

for $d=2$ and

$$\Delta_{nl}^{(3)} = n(n-2)(0.001\,40n^2 + 0.019\,92n + 0.034\,37) + l(l+1)$$
$$\times [-0.004\,20n^2 - 0.024\,21n + 0.002\,80\,l(l+1)$$
$$+ 0.050\,65] \quad (1.13b)$$

for $d=3$. Here, we have presented the $O(\varepsilon^3)$ results with improved accuracy in numerical coefficients and corrected a misprint in the expression for $d=3$ in Ref. [15]. No analytical formula for $\Delta_{nl}^{(3)}$ is available for general d, but the numerical result of the form (1.13) can be obtained for any given d. The large d limit is discussed in Sec. VI E.

Besides the calculational efficiency, an important advantage of the RG approach is its universality: it can also be applied to the case of finite correlation time or non-Gaussian advecting field; see Ref. [13]. For passively advected vector fields, any calculation of the exponents for higher-order correlations calls for the RG techniques already in the $O(\varepsilon)$ approximation [18–20]. Detailed introduction to the RG approach in the statistical theory of turbulence and the bibliography can be found in Refs. [21,22].

The main goal of this paper is to give the complete and detailed derivation of the third-order result (1.13) announced in Ref. [15], and to present and explain in detail the corresponding calculational technique. It might be useful not only for the rapid-change model (1.1)–(1.3) and its descendants, but also in a wider context of the statistical models of fully developed turbulence and critical dynamics.

Another scope of the paper is to discuss the nature and convergence properties of the ε expansion. The knowledge of the three terms allows one to obtain reasonable predictions for finite values of $\varepsilon \sim 1$ and to compare them with the existing nonperturbative results: analytical and numerical solutions of the zero-mode equations [6,7] and numerical simulations [23–25].

The plan of the paper is as follows. In Sec. II we recall the field theoretic formulation of the model, diagrammatic technique, renormalization, and RG equations. In Sec. III we briefly discuss the OPE, renormalization of composite operators (1.9) and their relationship to the issue of anomalous scaling. Since the ''ideology'' of the RG and OPE approach to the model (1.1)–(1.3) is explained in Refs. [10–13] in detail, here we confine ourselves to only the necessary information. In Sec. IV we present the general scheme of the calculation of the critical dimensions of the operators F_{nl}. In Sec. V, the calculation in the one-loop and two-loop approximations is presented in great detail. Section VI is devoted to the three-loop calculation; some results for the relevant quantities are given in the Appendix. In Sec. VII we discuss the convergence of the ε expansion, the improved inverse ε expansion, and comparison with existing nonperturbative results. The main ideas of the paper are briefly reviewed in the Conclusion.

II. FIELD THEORETIC FORMULATION OF THE MODEL, DIAGRAMMATIC TECHNIQUE, RENORMALIZATION, AND RG EQUATIONS

The stochastic problem (1.1)–(1.3) is equivalent to the field theoretic model of the set of three fields $\Phi \equiv \{\theta, \theta', \mathbf{v}\}$ with action functional
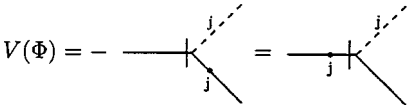
$$S(\Phi) = \theta' D_\theta \theta'/2 + \theta'[-\partial_t + \nu_0 \partial^2 - (v\,\partial)]\theta - \mathbf{v} D_v^{-1} \mathbf{v}/2. \tag{2.1}$$

The first four terms in Eq. (2.1) represent the Martin-Siggia-Rose-type action for the stochastic problem (1.1) and (1.2) at fixed $\mathbf{v}$, and the last term represents the Gaussian averaging over $\mathbf{v}$. Here D_θ and D_v are the correlators (1.2) and (1.3), respectively, the required integrations over $x = (t, \mathbf{x})$ and summations over the vector indices are understood.

The model (2.1) corresponds to a standard Feynman diagrammatic technique with the bare propagators vv, $\theta\theta$, $\theta\theta'$ (the line $\theta' \theta'$ is absent). In the diagrams, these propagators are represented by the lines

$$\langle vv \rangle_0 = \text{------} , \quad \langle \theta\theta \rangle_0 = \text{———} , \quad \langle \theta\theta' \rangle_0 = \text{———|} , \tag{2.2}$$

the slashed end of a solid line corresponds to the field θ', the end without a slash corresponds to θ. The triple vertex $V(\Phi) = -\theta' v_j \partial_j \theta = \partial_j \theta' v_j \theta$ [the equality holds due to the integration over $\mathbf{x}$ in Eq. (2.1)] is represented as

$$\tag{2.3}$$

The dot with the index j on the solid line denotes the differentiation $\partial/\partial x_j$ with respect to the argument $\mathbf{x}$ of the end of the line attached to the vertex; the index j of the derivative is contracted with the index of the end of the line vv attached to the vertex. Owing to the transversality of the vv line, the dot can be moved onto another line, as shown in Eq. (2.3). In the momentum representation, the vertex (2.3) corresponds to the factor $-ik_j$ or, equivalently, $+iq_j$, where $\mathbf{k}$ and $\mathbf{q}$ are the momenta flowing into the vertex via the fields θ' and θ, respectively. The sum of the three momenta flowing into the vertex via the fields θ, θ', v is equal to zero.

The line vv in the diagrams corresponds to correlation function (1.3), and the lines $\theta\theta'$ and $\theta\theta$ in model (2.1) in the $(\omega, \mathbf{k})$ representation correspond to the bare propagators

$$\langle \theta\theta' \rangle_0 = (-i\omega + \epsilon_\mathbf{k})^{-1}, \quad \langle \theta\theta \rangle_0 = C(\mathbf{k})(\omega^2 + \epsilon_\mathbf{k}^2)^{-1},$$

$$\epsilon_\mathbf{k} \equiv \nu_0 k^2, \tag{2.4}$$

where $C(\mathbf{k})$ is the Fourier transform of the function C from Eq. (1.2) and ω and $\mathbf{k}$ ''flow via the line from the left to the right'' if the standard form of the Fourier transform with respect to the coordinate and time differences is used.

In what follows, we shall work in the $(t, \mathbf{k})$ representation, where the propagators (2.4) have the forms

$$\langle \theta\theta' \rangle_0 = \Theta(t - t')\exp\{-(t - t')\epsilon_\mathbf{k}\}, \quad \langle \theta\theta \rangle_0$$

$$= \{C(\mathbf{k})/2\epsilon_\mathbf{k}\}\exp\{-|t - t'|\epsilon_\mathbf{k}\}; \tag{2.5}$$

in $\langle \theta\theta' \rangle_0$, t is the time argument of θ and t' is the argument of θ'.

The model (2.1) is logarithmic [the coupling constant g_0 in Eq. (1.4) is dimensionless] at $\varepsilon = 0$, and the UV divergences have the form of the poles in ε in the correlation functions of the fields θ, θ'. Superficial UV divergences, whose removal requires counterterms, are present only in the 1-irreducible function $\langle \theta'\theta \rangle_{\text{1-ir}}$, and the corresponding counterterm reduces to the form $\theta' \partial^2 \theta$; see Ref. [10]. Thus for the complete elimination of the UV divergences it is sufficient to perform the multiplicative renormalization of the parameters ν_0 and $g_0 = D_0/\nu_0$ with the only independent renormalization constant Z_ν,

$$\nu_0 = \nu Z_\nu, \quad g_0 = g\mu^\varepsilon Z_g,$$

$$Z_g = Z_\nu^{-1} \quad (D_0 = g_0\nu_0 = g\mu^\varepsilon \nu). \tag{2.6}$$

Here μ is the renormalization mass in the minimal subtraction (MS) scheme, which we always use in what follows, g and ν are renormalized analogs of the bare parameters g_0 and ν_0, and $Z = Z(g, \varepsilon, d)$ are the renormalization constants. In the MS scheme they have the form "1 + only poles in ε." The last relation in Eq. (2.6) results from the absence of renormalization of the contribution with D_v in Eq. (2.1).

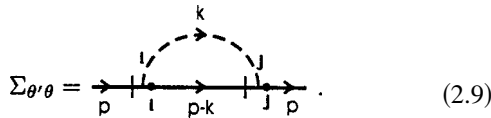The renormalized action is obtained from the functional (2.1) by the substitution (2.6) and has the form

$$S_R(\Phi) = \theta' D_\theta \theta'/2 + \theta'[-\partial_t + \nu Z_\nu \partial^2 - (v\partial)]\theta - \mathbf{v}D_v^{-1}\mathbf{v}/2,$$
(2.7)

where the amplitude $D_0 = g\mu^\varepsilon \nu$ from Eq. (1.3) is expressed in renormalized parameters using Eqs. (2.6).

The exact response function $G \equiv \langle \theta\, \theta' \rangle$ satisfies the standard Dyson equation, which in the $\omega, \mathbf{k}$ representation has the form

$$G^{-1}(\omega, \mathbf{p}) = -i\omega + \nu_0 p^2 - \Sigma_{\theta'\theta}(\omega, \mathbf{p}),$$
(2.8)

where the self-energy operator $\Sigma_{\theta'\theta}$ in the diagrammatic notation (2.2) and (2.3) is represented as follows:

$$\Sigma_{\theta'\theta} = \qquad .$$
(2.9)

The multiloop diagrams, which could be added on the right-hand side of Eq. (2.9), contain effectively closed circuits of retarded propagators $\langle \theta\, \theta' \rangle_0$ and therefore vanish; it is crucial here that the correlation function $\langle vv \rangle$ in Eq. (1.3) is proportional to the δ function in time. Therefore, the self-energy operator is given by the one-loop approximation exactly; it is independent of ω and has the form

$$\Sigma_{\theta'\theta}(\mathbf{p}) = -\frac{D_0 p_i p_j}{2(2\pi)^d} \int d\mathbf{k} P_{ij}(\mathbf{k}) N_k$$

$$= -\frac{D_0(d-1)p^2}{2d(2\pi)^d} \int d\mathbf{k} N_k \equiv -\frac{D_0(d-1)p^2}{2d} U,$$
(2.10)

where

$$U \equiv (2\pi)^{-d} \int d\mathbf{k} N_k = C_d \int_m^\infty dk\, k^{-1-\varepsilon} = C_d m^{-\varepsilon}/\varepsilon,$$

$$C_d \equiv S_d/(2\pi)^d$$
(2.11)

with N_k from Eq. (1.3). The quantity $S_d = 2\pi^{d/2}/\Gamma(d/2)$ is the surface area of the unit sphere in d-dimensional space. In Eq. (2.10) we have used the standard convention $\Theta(t-t') = 1/2$ at $t = t'$ for the step function in the $\theta\theta'$ line and the relation $\langle P_{ij}(\mathbf{k}) \rangle = \delta_{ij}(d-1)/d$ for the angular averaging of the transverse projector in d dimensions.

From the Dyson equation and Eqs. (2.10) and (2.11) it follows that the exact response function $\langle \theta\, \theta' \rangle$ is obtained from its bare counterpart $\langle \theta\, \theta' \rangle_0$ in Eqs. (2.4) and (2.5) simply by the replacement

$$\nu_0 \rightarrow \nu_{eff} \equiv \nu_0 + C_d(d-1)D_0 m^{-\varepsilon}/2d\varepsilon.$$
(2.12)

The renormalization constant Z_ν in Eq. (2.6) can be found exactly from the requirement that the "effective diffusivity" ν_{eff} be UV finite in renormalized theory (2.7), i.e., have no poles in ε when expressed in renormalized variables (2.6). In the MS scheme this gives

$$Z_\nu = 1 - u(d-1)/2d\varepsilon, \quad u \equiv g\, C_d, \quad C_d = S_d/(2\pi)^d,$$
(2.13)

where we have changed to the more convenient coupling constant u. In the renormalized variables, ν_{eff} is given by the expression

$$\nu_{eff} = \nu\left\{1 + \frac{u(d-1)[(\mu/m)^\varepsilon - 1]}{2d\varepsilon}\right\},$$
(2.14)

which is obviously finite at $\varepsilon \rightarrow 0$.

The basic RG equation for a multiplicatively renormalizable quantity $F = Z_F F_R$ (correlation function, composite operator, etc.) has the form

$$[\mathcal{D}_{RG} + \gamma_F]F_R = 0, \quad \mathcal{D}_{RG} = \mathcal{D}_\mu + \beta\partial_u - \gamma_\nu \mathcal{D}_\nu.$$
(2.15)

Here and below, $\mathcal{D}_x \equiv x\partial_x$ for any variable x, and the RG functions (the β function and the anomalous dimensions γ) are defined as

$$\beta \equiv \tilde{\mathcal{D}}_\mu u, \quad \gamma_F \equiv \tilde{\mathcal{D}}_\mu \ln Z_F = \beta\partial_u \ln Z_F \quad \text{for any } Z_F,$$
(2.16)

where $\tilde{\mathcal{D}}_\mu$ denotes the operation $\mu\partial_\mu$ at fixed bare parameters g_0, ν_0. From the definitions, the last relation in Eq. (2.6) and exact expression (2.13), for the basic RG functions one obtains

$$\beta(u) = u[-\varepsilon + \gamma_\nu], \quad \gamma_\nu = u(d-1)/2d.$$
(2.17)

From Eq. (2.17) it follows that the RG equations (2.15) possess an IR stable positive fixed point,

$$u_* = 2d\varepsilon/(d-1), \quad \beta(u_*) = 0, \quad \beta'(u_*) = \varepsilon > 0.$$
(2.18)

This fact implies that correlation functions of model (1.1)–(1.3) in the IR region ($\Lambda r \gg 1$, $mr \sim 1$) exhibit scaling behavior; the corresponding critical dimensions $\Delta[F] \equiv \Delta_F$ can be calculated as a series in ε. For the basic fields and quantities, including the composite operators θ^n, the dimensions are found exactly [10],

$$\Delta_\omega = 2 - \varepsilon, \quad \Delta_m = 1, \quad \Delta_\theta = (-1 + \varepsilon/2),$$

$$\Delta[\theta^n] = n\Delta_\theta, \quad \Delta_{\theta'} = d + 1 - \varepsilon/2$$
(2.19)

(no corrections of order ε^2 and higher). This is a consequence of the exact equality $\gamma_\nu(u_*) = \varepsilon$, which follows from Eqs. (2.17) and (2.18).

In particular, for the structure functions (1.5), relations (2.19) along with dimensionality considerations give

$$S_n(\mathbf{r}) = D_0^{-n/2} r^{n(1-\varepsilon/2)} \xi_n(mr), \qquad (2.20)$$

with some nontrivial dependence on the IR scale m contained in the scaling functions $\xi_n(mr)$.

III. COMPOSITE OPERATORS, OPERATOR PRODUCT EXPANSION, AND ANOMALOUS SCALING

Representations of the form (2.20) for any scaling functions $\xi(mr)$ describe the behavior of the correlation functions for $\Lambda r \gg 1$ and any fixed value of mr. The inertial range corresponds to the additional condition $mr \ll 1$. The form of the functions $\xi(mr)$ at $mr \to 0$ is studied using the OPE.

According to the OPE, the behavior of the quantities entering into the right-hand side of Eq. (1.5) for $\mathbf{r} = \mathbf{x} - \mathbf{x}' \to 0$ and fixed $\mathbf{x} + \mathbf{x}'$ is given by the infinite sum

$$[\theta(t,\mathbf{x}) - \theta(t,\mathbf{x}')]^n = \sum_F C_F(\mathbf{r}) F\left(t, \frac{\mathbf{x}+\mathbf{x}'}{2}\right), \qquad (3.1)$$

where C_F are coefficients regular in m^2 and F are all possible renormalized local composite operators allowed by the symmetry (more precisely, see below).

In what follows, it is assumed that the expansion (3.1) is made in irreducible tensors (scalars, vectors, and traceless tensors); the possible tensor indices of the operators F are contracted with the corresponding indices of the coefficients C_F. With no loss of generality, it can also be assumed that the expansion is made in "scaling" operators, i.e., those having definite critical dimensions Δ_F.

The structure functions (1.5) are obtained by averaging Eq. (3.1) with the weight $\exp \mathcal{S}_R$, the mean values $\langle F \rangle$ appear on the right-hand side. Their asymptotic behavior for $m \to 0$ is found from the corresponding RG equations (2.15) and has the form $\langle F \rangle \propto m^{\Delta_F}$.

From the RG representation (2.20) and the operator product expansion (3.1) we therefore find the following expression for the structure functions in the inertial range ($\Lambda r \gg 1$, $mr \ll 1$):

$$S_n(\mathbf{r}) = D_0^{-n/2} r^{n(1-\varepsilon/2)} \sum_F A_F(m\mathbf{r})(mr)^{\Delta_F}, \qquad (3.2)$$

with coefficients A_F regular in m^2.

Some general remarks are now in order.

Owing to translational invariance, the operators having the form of total derivatives give no contribution to Eq. (3.2): $\langle \partial F(x) \rangle = \partial \langle F(x) \rangle = \partial \times \text{const} = 0$.

In model (1.1)–(1.3), the operators with an odd number of fields θ also have vanishing mean values; their contributions vanish along with the odd structure functions themselves

(they will be "activated" in the presence of a nonzero mixed correlation function $\langle \mathbf{v}f \rangle$ or an imposed gradient of the scalar field).

If the function C in Eq. (1.2) depends only on $r = |\mathbf{r}|$, the model becomes SO(d) covariant and only the contributions of scalar operators enter into Eq. (3.2). Indeed, in the isotropic case the tensor indices of the mean values $\langle F \rangle$ of the operators F in Eq. (3.1) can only be those of Kronecker delta symbols. It is impossible, however, to construct a nonzero irreducible (traceless) tensor solely of the delta symbols.

In the presence of anisotropy, irreducible tensor operators acquire nonzero mean values and their contributions appear on the right-hand side of Eq. (3.2). In the simplest case of the uniaxial anisotropy, specified by a unit vector $\mathbf{n}$ in the correlation function (1.2), the mean value of a lth rank traceless operator is necessarily proportional to the lth rank symmetrical traceless tensor built of the vector $\mathbf{n}$ along with the delta symbols; its contraction with the corresponding coefficient A_F gives rise to the lth-order Legendre polynomial $P_l(z)$ with $z = (\mathbf{r} \cdot \mathbf{n})/r$. In general, the expansion in irreducible tensors in Eq. (3.1) after the averaging leads to the decomposition in the irreducible representations of SO(d), the lth sector corresponds to the contribution of the lth rank composite operators.

The leading term in the lth anisotropic sector is given by the lth rank tensor operator with minimal dimension $\Delta[F]$. The feature typical to the models describing turbulence is the existence of composite operators with *negative* critical dimensions; their contributions in the OPE lead to singular behavior of the scaling functions at $mr \to 0$, that is, to the anomalous scaling. The operators with minimal Δ_F are those involving the maximal possible number of fields θ and the minimal possible number of derivatives (at least for small ε). Both the problem (1.1)–(1.3) and the quantities (1.5) possess the symmetry $\theta \to \theta + \text{const}$. It then follows that the expansion (3.1) involves only operators invariant with respect to this shift and therefore built of the *gradients* of θ.

In general the operators entering into the right-hand side of Eq. (3.1) are those that appear in the Taylor expansion and those that admix to them in renormalization. The leading term of the Taylor expansion for S_n is the nth rank operator, which can symbolically be written as $(\partial \theta)^n$; its decomposition in irreducible tensors gives rise to operators of lower ranks. In the presence of the noise (1.2), operators of the form $(\partial \theta)^k$ with $k < n$ admix to them in renormalization and also appear in the OPE. Owing to the linearity of problem (1.1), operators with $k > n$ (whose contributions would be more important) do not admix to the terms of the Taylor expansion for S_n and do not appear in the corresponding OPE.

We thus conclude that the leading terms of the inertial-range behavior are related to the critical dimensions Δ_{nl} of the infinite family of irreducible tensor composite operators F_{nl} introduced in Eq. (1.9).

In general, operators (1.9) mix in renormalization. One can show that the corresponding infinite renormalization matrix
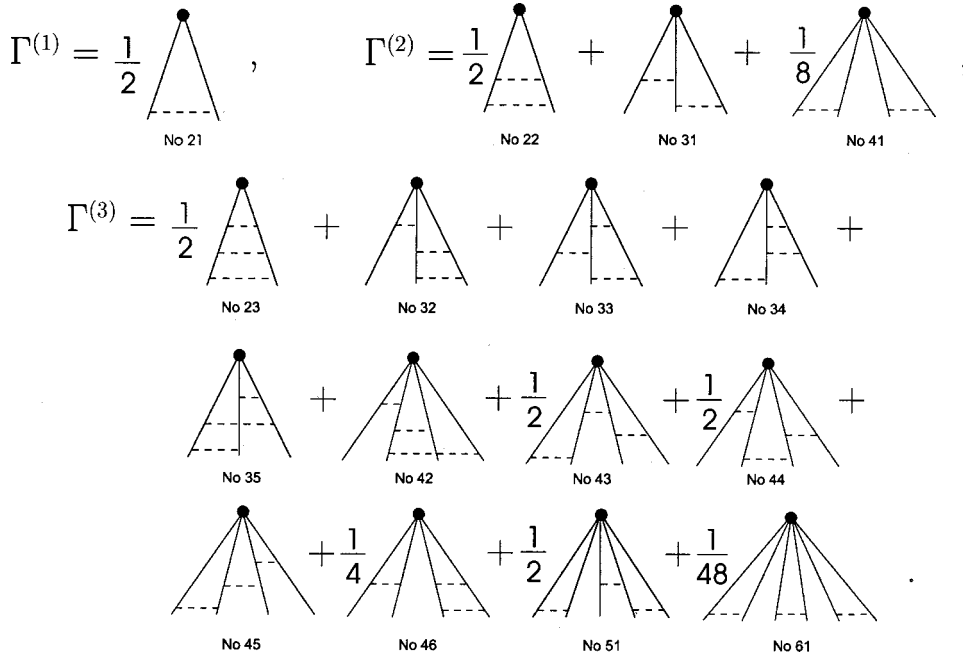
$$\Gamma^{(1)} = \frac{1}{2} \quad , \qquad \Gamma^{(2)} = \frac{1}{2} \quad + \quad + \quad \frac{1}{8} \quad ,$$

No 21   No 22   No 31   No 41

$$\Gamma^{(3)} = \frac{1}{2} \quad + \quad + \quad + \quad +$$

No 23   No 32   No 33   No 34

$$+ \quad + \frac{1}{2} \quad + \frac{1}{2} \quad +$$

No 35   No 42   No 43   No 44

$$+ \frac{1}{4} \quad + \frac{1}{2} \quad + \frac{1}{48} \quad .$$

No 45   No 46   No 51   No 61

FIG. 1. Diagrammatic representation of the function Γ in the three-loop approximation.

$$F_{nl} = \sum_{n'l'} Z_{nl,n'l'} F_{n'l'}^R \qquad (3.3)$$

is in fact block triangular, i.e., $Z_{nl,n'l'} = 0$ for $n' > n$, and so are the matrix of anomalous dimensions $\gamma(u) = Z^{-1} \tilde{\mathcal{D}}_\mu Z$ and the matrix of critical dimensions $\Delta = n + n\Delta_\theta + \gamma(u_*)$. It is then obvious that the dimensions Δ_{nl}, given by the eigenvalues of the latter matrix, are completely determined by the finite subblocks with $n' = n$. Therefore, we can neglect all the elements of the matrix (3.3) other than $Z_{nl,nl'}$. The latter are determined by the 1-irreducible correlation functions with one operator F_{nl} and n fields θ. The diagrams for such functions do not involve the propagator $\langle \theta \theta \rangle_0$ from Eq. (2.4) and can therefore be calculated directly in the "unforced" model without the noise (1.2), that is, without the first terms in the action functionals (2.1) and (2.7). In the absence of the forcing, the model becomes SO(d) covariant, the irreducible operators with different values of l cannot mix in renormalization, so that the blocks $Z_{nl,nl'}$ appear diagonal.

We thus conclude that the critical dimensions Δ_{nl} are determined by the diagonal elements $Z_{nl} \equiv Z_{nl,nl}$ of the matrix (3.3),

$$\Delta_{nl} = n + n\Delta_\theta + \gamma_{nl}(u_*) = n\varepsilon/2 + \gamma_{nl}(u_*), \quad \gamma_{nl}(u)$$

$$= \tilde{\mathcal{D}}_\mu \ln Z_{nl} = \beta \partial_u \ln Z_{nl} \qquad (3.4)$$

with β from Eq. (2.16), u_* from Eq. (2.18), and Δ_θ from Eq. (2.19). Owing to the renormalization, the critical dimension Δ_{nl} is not equal to the simple sum of critical dimensions $\Delta_\theta = (-1 + \varepsilon/2)$, $\Delta_\partial = 1$ of the fields and derivatives constituting F_{nl}. The elements Z_{nl} can be calculated in the model without forcing, in which the operators (1.9) are renormalized multiplicatively: $F_{nl} = Z_{nl} F_{nl}^R$.

IV. CALCULATION OF THE CRITICAL DIMENSIONS OF OPERATORS F_{nl}: GENERAL SCHEME

From now on, we shall consider composite operators (1.9) in the model without the noise, that is, with $D_\theta = 0$ in the action functional (2.1). They are renormalized multiplicatively, $F_{nl} = Z_{nl} F_{nl}^R$, and the renormalization constants $Z_{nl} = Z_{nl}(g, \varepsilon, d)$ are determined by the requirement that the 1-irreducible correlation function

$$\langle F_{nl}^R(x) \theta(x_1) \cdots \theta(x_n) \rangle_{\text{1-ir}} = Z_{nl}^{-1} \langle F_{nl}(x) \theta(x_1) \cdots \theta(x_n) \rangle_{\text{1-ir}}$$

$$\equiv Z_{nl}^{-1} \Gamma_{nl}(x; x_1, \ldots, x_n) \qquad (4.1)$$

be UV finite in renormalized theory (2.7), i.e., have no poles in ε when expressed in renormalized variables (2.6). This is equivalent to the UV finiteness of the product $Z_{nl}^{-1} \Gamma_{nl}(x; \theta)$, in which

$$\Gamma_{nl}(x; \theta) = \frac{1}{n!} \int dx_1 \cdots \int dx_n \Gamma_{nl}(x; x_1, \ldots, x_n)$$

$$\times \theta(x_1) \cdots \theta(x_n) \qquad (4.2)$$

is a functional of the field $\theta(x)$. In the zeroth approximation, the functional (4.2) coincides with the operator $F_{nl}(x)$, and in higher orders the kernel $\Gamma_{nl}(x; x_1, \ldots, x_n)$ is given by the sum of diagrams shown in Fig. 1. The analysis of the diagrams shows that for any argument x_s, the corresponding spatial derivative is isolated as an external factor from each diagram. Using the integration by parts, these derivatives can be moved onto the corresponding fields $\theta(x_s)$ in Eq. (4.2), so that the quantity (4.2) can be represented as a functional of the vector field $w_i \equiv \partial_i \theta$,

$$\Gamma_{nl}(x;\theta)=\frac{1}{n!}\int dx_1\cdots\int dx_n\tilde{\Gamma}_{nl}^{i_1\cdots i_n}(x;x_1,\ldots,x_n)$$

$$\times w_{i_1}(x_1)\cdots w_{i_n}(x_n). \tag{4.3}$$

The diagrams that determine the kernel $\tilde{\Gamma}$ in Eq. (4.3) contain only logarithmic UV divergencies. Therefore, in order to find the constant Z_{nl}^{-1} it is sufficient to calculate the functional $\tilde{\Gamma}$ with some special choice of its functional argument w_i, namely, one can replace it by its value at the fixed point x, the argument of the operator F_{nl} in Eqs. (4.1). Now the product $w_{i_1}(x)\cdots w_{i_n}(x)$ can be taken outside the integrals over $x_1,\ldots,x_n$ in Eq. (4.3), so that the functional $\Gamma_{nl}(x;\theta)$ turns to a local composite operator. The integration of the remaining function $\tilde{\Gamma}_{nl}$ over $x_1,\ldots,x_n$ gives a quantity independent of any coordinate variables, and its vector indices can only be those of Kronecker delta symbols. Their contraction with the indices of the product $w_{i_1}(x)\cdots w_{i_n}(x)$ gives rise to the original operator $F_{nl}(x)$ with some scalar coefficient $\bar{\Gamma}$. The integration over $x_1,\ldots,x_n$ means that in the Fourier representation, the corresponding correlation function is calculated with all its momenta set equal to zero, which is always implied in what follows.

Now we turn to the derivation of practical formulas for the calculation of the constants Z_{nl}^{-1} from the diagrams. For the sake of brevity, we introduce the notation,

$$Z_{nl}\equiv Z_F,\quad F_{nl}(x)\equiv F,\quad \Gamma_{nl}(x;\theta)\equiv\Gamma=F\bar{\Gamma}. \tag{4.4}$$

Then the UV finiteness of the quantity $Z_{nl}^{-1}\Gamma_{nl}(x;\theta)$ is expressed by the relation

$$P_{\text{div}}[Z_F^{-1}\Gamma]=0, \tag{4.5}$$

where P_{div} is the operation that selects the UV divergent part; in the MS scheme, it selects only poles in ε. Classifying the contributions in model (2.7) according to the powers of the renormalized coupling constant u from Eq. (2.13) gives

$$Z_F^{-1}=1+\sum_{k=1}^{\infty}[Z_F^{-1}]_k,\quad \Gamma=\sum_{k=0}^{\infty}\Gamma_k=F+F\sum_{k=1}^{\infty}\bar{\Gamma}_k, \tag{4.6}$$

where $[Z_F^{-1}]_k$, Γ_k, and $\bar{\Gamma}_k$ are the contributions of order u^k in the respective quantities. We substitute expressions (4.6) into Eq. (4.5) and omit the overall factor F; this gives

$$P_{\text{div}}\left[Z_F^{-1}+Z_F^{-1}\sum_{k=1}^{\infty}\bar{\Gamma}_k\right]=0. \tag{4.7}$$

We recall that in the MS scheme one has ''$Z_F^{-1}=1+$ only poles in ε,'' so that $P_{\text{div}}\{Z_F^{-1}\}=Z_F^{-1}-1$. Substituting this equality into Eq. (4.7) gives the relation

$$Z_F^{-1}=1-P_{\text{div}}\left[Z_F^{-1}\sum_{k=1}^{\infty}\bar{\Gamma}_k\right], \tag{4.8}$$

which allows for the recurrent calculation of the contributions $[Z_F^{-1}]_k$ in the expansion (4.6) from the quantities $\bar{\Gamma}_k$. Indeed, selecting in Eq. (4.8) terms of the same order in u gives

$$[Z_F^{-1}]_1=-P_{\text{div}}\{\bar{\Gamma}_1\}, \tag{4.9a}$$

$$[Z_F^{-1}]_2=-P_{\text{div}}\{\bar{\Gamma}_2+[Z_F^{-1}]_1\bar{\Gamma}_1\}, \tag{4.9b}$$

$$[Z_F^{-1}]_3=-P_{\text{div}}\{\bar{\Gamma}_3+[Z_F^{-1}]_1\bar{\Gamma}_2+[Z_F^{-1}]_2\bar{\Gamma}_1\}, \tag{4.9c}$$

and so on. The relations given in Eq. (4.9) are sufficient for the three-loop calculation.

In Fig. 1, we present, along with respective symmetry coefficients, all the diagrams needed for the three-loop calculation of the function Γ, except for those with the self-energy insertions of the form (2.9) in the $\theta\theta'$ lines. (The symmetry coefficients that are not shown are equal to unity.) The index l in $\Gamma^{(l)}$ denotes the number of loops (that is, independent integration momenta): $l=1,2,3$. Below each diagram we give its number, which will always be used in the following to refer to a diagram. The numbers have the forms ''No. XY,'' where X is the number of ''rays'' in the diagram and Y is the order number (from the left to the right in Fig. 1) of the diagram in the subset with given X.

The thick dots in the diagrams correspond to the vertices of the composite operator F (more precisely, see below), all the horizontal dashed lines correspond to correlation functions $\langle vv\rangle$ from Eq. (1.3) with $D_0=g\nu\mu^\varepsilon$, and the rays correspond to chains of lines $\langle\theta\theta'\rangle_0\langle\theta\theta'\rangle_0\cdots$ in the same order on each ray: the upper end of each line corresponds to the field θ and the lower end corresponds to θ'. For this reason, in contrast with Eq. (2.9), in Fig. 1 we do not add slashes at the ends of the lines. If desired, they can easily be restored: a slash should be added in the lower end of each line belonging to a ray. The lowest ''external lines'' of the diagrams in Fig. 1 correspond to the factors θ (and not to the propagators). We also note that the diagrams in Fig. 1 do not involve the $\theta\theta$ lines (even in the presence of the noise).

In Fig. 1, we omitted the diagrams that are topologically possible and would be needed for the general correlation function (1.3), but in our model with the delta function in time in Eq. (1.3) they vanish due to the presence of the closed circuits of retarded propagators $\langle\theta\theta'\rangle_0$; cf. the remark in Sec. II below Eq. (2.9).

The contributions of the diagrams with the self-energy insertions (2.9) will automatically be included if the propagators $\langle\theta\theta'\rangle_0$ in Fig. 1 are taken to be exact, that is, with $\epsilon_{\mathbf{k}}=\nu_{eff}k^2$ in Eqs. (2.4) and (2.5). In the renormalized variables, ν_{eff} is given by Eq. (2.14), the zero-order approximation being $\nu_{eff}=\nu$. It is easy to see that the parameter ν from $\epsilon_{\mathbf{k}}=\nu k^2$ enters into the final answers for the diagrams as ν^{-l}, where l is the number of loops in the diagram. It is thus

sufficient to calculate the diagrams without the self-energy insertions and with $\epsilon_{\mathbf{k}} = \nu k^2$ and then introduce the additional factor

$$(\nu_{eff}/\nu)^{-l} = [1+Q]^{-l}, \quad Q = \frac{u(d-1)[(\mu/m)^\varepsilon - 1]}{2d\varepsilon}$$
$$(4.10)$$

for any l-loop diagram; see Eq. (2.14). We stress that the replacement $\nu \to \nu_{eff}$ is not needed in the amplitude $D_0 = g\nu\mu^\varepsilon$ of the correlation function (1.3).

Expression (2.14) corresponds to the special choice of the function N_k in Eq. (1.3). If the specific form of the IR regularization is different [for example, the function $N_k = (k^2 + m^2)^{-d/2-\varepsilon/2}$ was used in Refs. [5,10]], the relation (2.10) for $\Sigma_{\theta'\theta}$ remains valid, but the explicit form of the integral U in Eq. (2.11) changes. Then the quantity Q in Eq. (4.10) is given by the following general relation:

$$Q = -[\Sigma_{\theta'\theta} - P_{\text{div}}\Sigma_{\theta'\theta}]/\nu p^2, \qquad (4.11)$$

which recovers the expression (4.10) for N_k from Eq. (1.3).

Introduction of the additional factors (4.10) to the diagrams of $\Gamma^{(l)}$ in Fig. 1 with $D_0 = g\nu\mu^\varepsilon$ in Eq. (1.3) and $\epsilon_{\mathbf{k}} = \nu k^2$ in Eq. (2.5) for the quantities $\bar\Gamma_n$ in Eq. (4.9) gives

$$\bar\Gamma_1 = \bar\Gamma^{(1)}, \quad \bar\Gamma_2 = \bar\Gamma^{(2)} - Q\,\bar\Gamma^{(1)},$$

$$\bar\Gamma_3 = \bar\Gamma^{(3)} - 2Q\,\bar\Gamma^{(2)} + Q^2\bar\Gamma^{(1)}. \qquad (4.12)$$

Expanding the quantity Q from Eq. (4.10) in ε gives rise to contributions with the logarithms $\ln(\mu/m)$; similar contributions also come from the factors $(\mu/m)^{l\varepsilon}$, which naturally arise in any l-loop diagram in $\Gamma^{(l)}$. It is well known that the renormalization constants in the MS scheme are independent of any mass parameters, like m and μ in the case at hand. This means that, after the substitution of relations (4.12) into Eqs. (4.9), all contributions with $\ln(\mu/m)$ in Z_F^{-1} will cancel each other. Such cancellation provides a good possibility to control the absence of calculational errors. In the two-loop calculation [10] we have checked the cancellation of the contributions $\varepsilon^{-1}\ln(\mu/m)$ in $[Z_F^{-1}]_2$. There, the function N_k was taken in the form different from Eq. (1.3) (see above), the ε expansion of the corresponding quantity Q in Eq. (4.11) contained constant terms along with powers of the logarithms $\ln(\mu/m)$, so that it was necessary to take into account the contribution with Q in expression (4.12) for $\bar\Gamma_2$.

Our present choice for N_k in Eq. (1.3) is much more convenient, because the corresponding integral (2.11) contains only poles in ε, and the ε expansion of the corresponding quantity Q in Eq. (4.10) contains only powers of $\ln(\mu/m)$ with no constant contributions. Since we know in advance that all contributions with $\ln(\mu/m)$ in Z_F^{-1} will cancel each other, we may simply set $\mu = m$ in the calculation of this quantity. Then all the contributions with $\ln(\mu/m)$ vanish, in Eq. (4.10) we obtain $Q = 0$ (no corrections from the self-energy insertions are needed), in Eq. (4.12) we obtain $\bar\Gamma_l = \bar\Gamma^{(l)}$, and the factors $(\mu/m)^{l\varepsilon}$ in the l-loop diagrams turn to

unity. In what follows, in the calculations of the diagrams in $\bar\Gamma^{(l)}$ we shall retain the factors $(\mu/m)^{l\varepsilon}$ and replace them with unity only in the last step, that is, in the calculation of Z_F^{-1}.

Let us turn to the vertex of the composite operator F, denoted in Fig. 1 by thick dots on the top of the diagrams. According to the general rules of the universal diagrammatic technique (see, e.g., Ref. [26]), for any composite operator $F(x)$ built of the fields θ, the vertex with $k \geq 0$ attached lines corresponds to the vertex factor

$$V_k(x;x_1,\cdots,x_k) \equiv \delta^k F(x)/\delta\,\theta(x_1)\cdots\delta\,\theta(x_k).$$
$$(4.13)$$

The arguments $x_1 \cdots x_k$ of the quantity (4.13) are contracted with the arguments of the upper ends of the lines $\theta\,\theta'$ attached to the vertex. For our operators (1.9), built solely of the gradients $w_i(x) = \partial\theta(x)/\partial x_i$ at a single spacetime point x, the factors (4.13) contain the product $\partial_{i_1}\delta(x-x_1)\cdots\partial_{i_k}\delta(x-x_k)$, and the integrations over $x_1\cdots x_k$ are easily performed: the derivatives move onto the upper ends of the corresponding lines $\theta\,\theta'$ attached to the vertex (such derivatives we denote by dots on the lines), and their arguments $x_1\cdots x_k$ are substituted with x. After the derivatives have been moved inside the diagram, the remaining vertex factor for the operator $F(x)$ can be understood as a usual derivative,

$$V_{i_1\cdots i_k}(x) = \partial^k F(x)/\partial w_{i_1}(x)\cdots\partial w_{i_k}(x). \qquad (4.14)$$

In what follows, in order to simplify the notation we shall omit the argument x and use the numerical indices $1,\ldots,k$ instead of $i_1\cdots i_k$. Then the vertex factor (4.14) for a k-ray diagram takes on the form

$$V_{12\ldots} = \partial_1\partial_2\cdots F \quad \text{with} \quad \partial_i \equiv \partial/\partial w_i. \qquad (4.15)$$

Diagrams Nos. 41, 46, 51, 61 in Fig. 1 are ''factorizable'' in the sense that they can be reduced to the products of blocks with a lesser number of rays. All the other diagrams in Fig. 1 will be termed ''normal.''
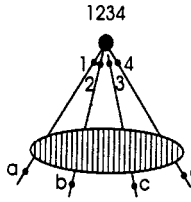
A. Scalarization of the diagrams

The contribution of a specific diagram into the functional Γ in Eq. (4.3) for any composite operator F, built of the gradients $w_i = \partial_i\theta$, is represented in the form

$$\Gamma = V_{12\ldots}I^{ab\cdots}_{12\cdots}w_a w_b\cdots, \qquad (4.16)$$

where $V_{12\ldots}$ is the vertex factor (4.15), $I^{ab\cdots}_{12\cdots}$ is the ''internal block'' of the diagram with free indices, the product $w_a w_b\cdots$ corresponds to external lines. The numerical indices $1,2,\ldots$ will always be understood as $i_1,i_2,\ldots,$ their number in Eq. (4.16) equals the number of the letter indices $a,b,\ldots$ and is determined by the number of ''rays,'' that is, the number of lines that attach to the vertex of the operator. These lines are given by products of the propagators $\langle\theta\,\theta'\rangle_0$ from Eq. (2.5) with $\epsilon_{\mathbf{k}} = \nu k^2$ (see above) and are connected

by the lines vv from Eq. (1.3). As an example, we present the general form of a four-ray diagram Γ,

$$= V_{1234}\, I^{abcd}_{1234}\, w_a w_b w_c w_d. \qquad (4.17)$$

The thick dot on the top represents the vertex of the composite operator, it corresponds to the vertex factor V_{1234} in Eq. (4.15). The dots on the lines denote the differential operation $\partial_i \equiv \partial/\partial x_i$; their indices are shown explicitly in the diagram. The lower external lines of the diagram correspond to factors θ; the derivatives at the external vertices (2.3), denoted by dots with the indices a,b,c,d, act on these fields and turn them into the product $w_a w_b w_c w_d$ with $w_i \equiv \partial\theta/\partial x_i$. After all these differentiations have been performed, all the external momenta in the diagrams are set to zero; the IR regularization is provided by the parameter m in the function $\langle vv \rangle$ from Eq. (1.3).

The diagrams are calculated in the time-momentum representation. The integration momenta are assigned to all internal lines; the number of independent momenta is equal to the number of vv lines. The dots with the numerical indices $1,2,\ldots$ on the upper lines in Eq. (4.17) correspond to the vector factors $\pm ik_s$, coming from the vertex of the composite operator. Here **k** is the integration momentum flowing via the line with the index shown near the dot ($s=1,2,3,4$); the coefficient equals $-i$ if the momentum "flows into the dot" and $+i$ if the momentum "flows out." In general, similar factors are also present inside the diagram, that is, inside the shaded block in Eq. (4.17). Collecting all such factors $\pm i$ from the whole diagram gives a certain "sign factor" ± 1, which, of course, should be taken into account in the calculations.

Since the vertex factor (4.15) and the product $w_a w_b \cdots$ are symmetrical with respect to any permutations of their indices, the quantity $I^{ab\cdots}_{12\ldots}$ in Eq. (4.16) is automatically symmetrized with respect to any permutations of the letter indices $a,b,\ldots$ and the numerical indices $1,2,\ldots$. In what follows, such symmetrization will always be denoted by the symbol $\mathcal{S}$.

For any fixed number of rays k, the quantity $\mathcal{S}I$ is represented as a linear combination

$$\mathcal{S}I = \sum_i B_i S_i \qquad (4.18)$$

of certain basis tensor structures $S_i = (S_i)^{ab\cdots}_{1,2,\ldots}$ with certain numerical coefficients B_i. The structures for the k-ray diagrams with $k=2,3,4$ have the forms (there are two structures for $k=2,3$ and three structures for $k=4$)

$$k=2, \quad S_1 = \mathcal{S}[\delta_{1a}\delta_{2b}], \quad S_2 = \mathcal{S}[\delta_{12}\delta_{ab}];$$

$$k=3, \quad S_1 = \mathcal{S}[\delta_{1a}\delta_{2b}\delta_{3c}], \quad S_2 = \mathcal{S}[\delta_{12}\delta_{ab}\delta_{3c}];$$

$$k=4, \quad S_1 = \mathcal{S}[\delta_{1a}\delta_{2b}\delta_{3c}\delta_{4d}],$$

$$S_2 = \mathcal{S}[\delta_{12}\delta_{ab}\delta_{3c}\delta_{4d}], \quad S_3 = \mathcal{S}[\delta_{12}\delta_{34}\delta_{ab}\delta_{cd}]. \qquad (4.19)$$

This is sufficient for the three-loop calculation, because the diagrams with $k=5,6$ in Fig. 1 factorize into products of the blocks with $k=2,3$.

The quantities that will be directly calculated from the diagrams are not the coefficients B_i themselves, but the following scalar quantities related to them:

$$A_i = \mathrm{tr}[(S_i)^{ab\cdots}_{1,2,\ldots}\mathcal{S}I^{ab\cdots}_{12\cdots}] = \mathrm{tr}[S_i\mathcal{S}I]. \qquad (4.20)$$

Here and below, the symbol tr denotes the contraction with respect to all repeated indices, which will not be shown explicitly.

It is therefore necessary to express the coefficients B_i in Eq. (4.18) in terms of the quantities (4.20). This is easily done: substituting Eq. (4.18) into Eq. (4.20) gives

$$A_i = \sum_k M_{ik} B_k,$$

where

$$M_{ik} \equiv \mathrm{tr}[S_i S_k]. \qquad (4.21)$$

In a compact notation, $A = MB$ (matrix M acts onto vector B and gives vector A). The symmetrical matrix M defined in Eq. (4.21) is easily calculated for any given set of structures of the form (4.19); then the corresponding inverse matrix M^{-1} is found and the desired expressions for B in terms of A follow from the relation $B = M^{-1}A$.

Below we give the explicit expressions for matrix elements $M_{ik} = M_{ki}$ for the structures (4.19),

$$k=2, \quad M_{11} = d(d+1)/2, \quad M_{12} = d, \quad M_{22} = d^2;$$

$$k=3, \quad M_{11} = d(d+1)(d+2)/6, \quad M_{12} = d(d+2)/3,$$

$$M_{22} = d(d+2)^2/9;$$

$$k=4, \quad M_{11} = d(d+1)(d+2)(d+3)/24,$$

$$M_{12} = d(d+2)(d+3)/12, \quad M_{13} = d(d+2)/3,$$

$$M_{22} = d(d+2)(d^2+7d+16)/72,$$

$$M_{23} = d(d+2)^2/9, \quad M_{33} = d^2(d+2)^2/9. \qquad (4.22)$$

It is worth noting that in the calculation of quantities like M_{ik} in Eq. (4.21) or A_i in Eq. (4.20), it is sufficient to retain the symbol $\mathcal{S}$ only in one of the cofactors, because the second is symmetrized automatically and can be replaced with one of its terms, like the expressions in square brackets in Eq. (4.19).

Inverting the matrices M in Eq. (4.22) gives the following explicit expressions of the coefficients B in terms of A:

$$k=2, \quad B_1 = 2\alpha[dA_1 - A_2],$$

$$B_2 = \alpha[-2A_1 + (d+1)A_2] \quad \text{with}$$

$$\alpha \equiv [(d-1)d(d+2)]^{-1}, \tag{4.23a}$$

$$k=3, \quad B_1 = 6\alpha[(d+2)A_1 - 3A_2],$$

$$B_2 = 9\alpha[-2A_1 + (d+1)A_2] \quad \text{with}$$

$$\alpha \equiv [(d-1)d(d+2)(d+4)]^{-1}, \tag{4.23b}$$

$$k=4, \quad B_1 = 24\alpha[(d+2)(d+4)A_1 - 6(d+2)A_2 + 3A_3],$$

$$B_2 = 72\alpha[-2(d+2)A_1 + (d^2+3d+6)A_2 - (d+3)A_3],$$

$$B_3 = 9\alpha[8A_1 - 8(d+3)A_2 + (d+3)(d+5)A_3] \quad \text{with}$$

$$\alpha \equiv [(d-1)d(d+1)(d+2)(d+4)(d+6)]^{-1}. \tag{4.23c}$$

It should be emphasized that the above relations (4.22) and (4.23) are independent of the specific choice of a composite operator built of the gradients $w_i = \partial_i \theta$, which only determines the explicit form of the vertex factor (4.15).

B. Contractions of basic tensor structures

Consider the procedure of the contraction of the quantities $I^{ab\cdots}_{12\cdots}$ in Eq. (4.16) with external factors: the vertex factor $V_{12\cdots}$ of the composite operator and the product $w_a w_b \cdots$. General rules given below are valid for any local monomial F built of the gradients $w_i = \partial_i \theta$. The operator F may have vector indices; as a rule, they will not be shown explicitly.

Substituting the decomposition (4.18) into Eq. (4.16) gives

$$\Gamma = \sum_i B_i V_{12\cdots}(S_i)^{ab,\cdots}_{1,2,\cdots} w_a w_b \cdots = \sum_i B_i \Gamma_i, \tag{4.24}$$

where Γ_i are the contractions of the quantities (4.19) with the external factors

$$\Gamma_i = V_{12\cdots}(S_i)^{ab,\cdots}_{1,2,\cdots} w_a w_b \cdots. \tag{4.25}$$

Consider first the contractions

$$(T_i)_{12\cdots} = (S_i)^{ab,\cdots}_{1,2,\cdots} w_a w_b \cdots \tag{4.26}$$

of the structures S_i with the external factors w. For quantities (4.19), they are easily calculated,

$$k=2, \quad (T_1)_{12} = w_1 w_2, \quad (T_2)_{12} = w^2 \delta_{12};$$

$$k=3, \quad (T_1)_{123} = w_1 w_2 w_3, \quad (T_2)_{123} = w^2 \mathcal{S}[\delta_{12} w_3];$$

$$k=4, \quad (T_1)_{1234} = w_1 w_2 w_3 w_4,$$

$$(T_2)_{1234} = w^2 \mathcal{S}[\delta_{12} w_3 w_4], \quad (T_3)_{1234} = w^4 \mathcal{S}[\delta_{12} \delta_{34}], \tag{4.27}$$

where the symbol $\mathcal{S}$ denotes the symmetrization with respect to the *numerical* indices.

From Eqs. (4.25) and (4.26) one obtains

$$\Gamma_i = V_{12\cdots}(T_i)_{12\cdots}, \tag{4.28}$$

where the symbol $\mathcal{S}$ in the quantities (4.27) can be omitted owing to the fact that the vertices $V_{12\cdots}$ are symmetrical.

For a general k-ray diagram we need to calculate contractions of the vertex factors $V_{1\cdots k}$ with the structures $T_{1\cdots k}$ of the form (4.27). Their basis is provided by the set

$$w_1 \cdots w_k, \quad w^2 \delta_{12} w_3 \cdots w_k,$$

$$w^4 \delta_{12} \delta_{34} w_5 \cdots w_k, \quad \text{and so on.} \tag{4.29}$$

Consider first the contraction of the vertex factor (4.15) with the first monomial in Eq. (4.29), that is, the expression $L_k F$ with the operator

$$L_k \equiv w_1 \cdots w_k \partial_1 \cdots \partial_k, \quad \partial_i \equiv \partial/\partial w_i. \tag{4.30}$$

The key role in the calculation of the quantity $L_k F$ is played by the following consideration: by permutations of the factors w and $\partial/\partial w$, the operator L_k in Eq. (4.30) can be represented in the form of a polynomial in the operation $\mathcal{D} \equiv w_i \partial/\partial w_i$. The action of the latter onto any monomial F is easily found, namely, $\mathcal{D}F = nF$, where n is the total number of the fields w in the monomial F. By permutations of the factors w and $\partial/\partial w$, one can easily obtain the recurrent relation $L_{k+1} = L_k(\mathcal{D}-k)$ for the operator L_k, which along with the relation $L_1 = \mathcal{D}$ gives

$$L_k = \mathcal{D}(\mathcal{D}-1)(\mathcal{D}-2)\cdots(\mathcal{D}-k+1), \quad \mathcal{D} \equiv w_i \partial/\partial w_i. \tag{4.31}$$

When this operation acts onto F, each symbol $\mathcal{D}$ is replaced with the number n, which gives the desired coefficient

$$L_k F = n(n-1)(n-2)\cdots(n-k+1)F, \tag{4.32}$$

where n is the total number of the factors w in the operator F.

Consider now the contraction of the vertex factor (4.15) with the second structure in Eq. (4.29). The latter includes the factor δ_{12}, which after the contraction with $\partial_1 \partial_2$ gives the Laplace operator $\partial^2 \equiv \partial_i \partial_i$ with $\partial_i \equiv \partial/\partial w_i$. This operator commutes with the other derivatives ∂_i and acts directly onto F. Therefore the first task is the calculation of the quantity $\partial^2 F$, which is easily done for any specific monomial F built of the gradients $w_i = \partial_i \theta$.

From now on, we shall confine ourselves with the family of operators F_{nl} from Eq. (1.9), which in the new notation take on the form

$$F_{nl} = \mathcal{P}_{\text{ir}}[w_1 \cdots w_l w^{2p}], \quad n = l + 2p. \tag{4.33}$$

The quantities $\partial^2 F$ for such operators are easily calculated,

$$\partial^2 F_{nl} = \lambda_{nl} F_{n-2,l}, \quad \lambda_{nl} = (n-l)(d+n+l-2). \tag{4.34}$$
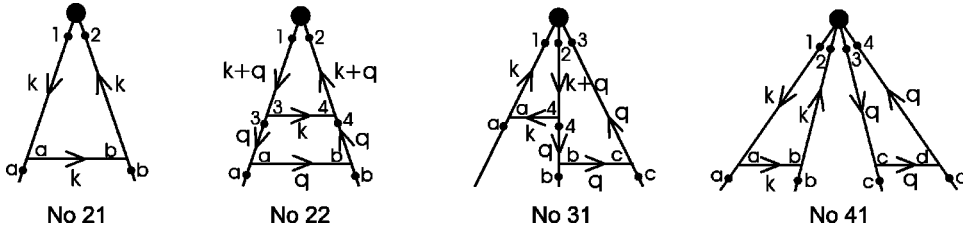
FIG. 2. Diagrams of the function Γ in the one-loop and two-loop approximations in the detailed notation.

It is worth noting that in the calculation of the quantity $\partial^2 F$, there is no need to take into account contributions in which both derivatives act onto the monomial $w_1 \cdots w_l$ in Eq. (4.33): in this case, two factors w are necessarily replaced with the symbol δ_{is} (the number of free indices is preserved, and the number of factors w is reduced by two under the action of ∂^2), and any contribution with δ_{is} disappears under the action of the operation $\mathcal{P}_{\mathrm{ir}}$ in Eq. (4.33).

It is clear that the combination of the relations (4.32) and (4.34) gives a complete solution to the problem of the calculation of the contractions of vertex factor (4.15) with basis structures of the form (4.29) for our specific operators (4.33), and that the above considerations can be directly generalized to the case of any operator F polynomial in w. If the basis structure includes several delta symbols [e.g., two delta symbols in the third monomial in Eq. (4.29)], the operation ∂^2 should be applied repeatedly; one should also remember that each next Laplacian acts onto the operator that has already been modified [replacement $n \rightarrow n-2$ in Eq. (4.34)]. After all the operations ∂^2 have been applied, only the operation L_k, Eq. (4.30), with the reduced number of factors remains; it acts onto the properly modified operator F according to the rule (4.32). For our operators F_{nl}, additional scalar factors $w^2, w^4, \ldots$ in monomials (4.29) restore the original scalar factor w^{2p} in Eq. (4.33). Therefore, all the quantities Γ_i in Eq. (4.28) are proportional to the original operator (4.33): $\Gamma_i = k_i F$ with some numerical coefficients k_i. They are easily found using the rules discussed above. In particular, for the two-ray diagrams $\Gamma_1 = V_{12} w_1 w_2 = L_2 F = n(n-1)F$, $\Gamma_2 = V_{12} w^2 \delta_{12} = w^2 \partial^2 F = \lambda_{nl} F$, and similarly for the three-ray and four-ray diagrams.

Substituting the relation $\Gamma_i = k_i F$ into Eq. (4.24) gives

$$\Gamma = F \bar{\Gamma}, \quad \bar{\Gamma} = \sum_i k_i B_i, \qquad (4.35)$$

where k_i are the coefficients in front of F in the contractions of the vertex factor $V_{1 \ldots k}$ with structures (4.29), numbered in the same order (k_1 corresponds to the structure without delta symbols, k_2 corresponds to the structure with one delta symbol, and so on),

$$k=2, \quad k_1 = n(n-1), \quad k_2 = \lambda_{nl},$$

where

$$\lambda_{nl} = (n-l)(d+n+l-2); \qquad (4.36a)$$

$$k=3, \quad k_1 = n(n-1)(n-2), \quad k_2 = (n-2)\lambda_{nl}; \qquad (4.36b)$$

$$k=4, \quad k_1 = n(n-1)(n-2)(n-3),$$

$$k_2 = (n-2)(n-3)\lambda_{nl}, \quad k_3 = \lambda_{n-2,l}\lambda_{nl}; \qquad (4.36c)$$

$$k=5, \quad k_1 = n(n-1)(n-2)(n-3)(n-4),$$

$$k_2 = (n-2)(n-3)(n-4)\lambda_{nl}, \quad k_3 = (n-4)\lambda_{n-2,l}\lambda_{nl}; \qquad (4.36d)$$

$$k=6, \quad k_1 = n(n-1)(n-2)(n-3)(n-4)(n-5),$$

$$k_2 = (n-2)(n-3)(n-4)(n-5)\lambda_{nl},$$

$$k_3 = (n-4)(n-5)\lambda_{n-2,l}\lambda_{nl}, \quad k_4 = \lambda_{n-4,l}\lambda_{n-2,l}\lambda_{nl}. \qquad (4.36e)$$

The coefficients k_i with $k=5$ and 6 will be needed only for the calculation of the factorizable diagrams Nos. 51, 61 with five and six rays, repectively.

The quantities A_i are calculated directly from the diagrams, then one calculates the quantities B_i using the relations (4.23), and then, finally, one calculates the desired contribution of the diagram Γ using the relations (4.35) and (4.36).

C. Calculation of the quantities A_i

The quantities $I_{12\cdots}^{ab\cdots}$ for the diagrams Γ are calculated at zero external momenta; the independent integration momenta will always be denoted by $\mathbf{k}$ in the one-loop diagrams, $\mathbf{k}, \mathbf{q}$ in all two-loop diagrams, and $\mathbf{k}, \mathbf{q}, \mathbf{l}$ in all three-loop diagrams. They are always assigned to the horizontal lines vv; in the normal (not factorizable) diagrams the order is the following: $\mathbf{k}$ flows via the uppermost line, $\mathbf{q}$ flows via the next line, and $\mathbf{l}$ flows via the lowest line.

These rules are illustrated by Fig. 2, where the one-loop and two-loop diagrams are presented with all their momenta; the directions of the latter are shown by arrows. We denote all the propagators by solid lines because the horizontal vv lines cannot be confused with the "rays" built of the $\theta \theta'$ lines. The letter indices $a, b, \ldots$ of the vv lines are always free (they will be contracted with the indices of the external factors $w_a w_b \cdots$), while the numerical indices of the vv lines are always contracted with the indices of derivatives (that is, the momentum factors $\pm i p_s$), shown by dots on the $\theta \theta'$ lines.

We shall calculate the diagrams in the time-momentum $(t, \mathbf{k})$ representation. First, the elementary integrations over all times are performed. This gives a certain "energy denominator" ϕ_E, that is, the factor ϕ_E^{-1} in the integrand. The remaining integrations are those over d-dimensional mo-

menta ($\mathbf{k}$ in one-loop diagrams, $\mathbf{k}$, $\mathbf{q}$ in two-loop diagrams, and $\mathbf{k}$, $\mathbf{q}$, $\mathbf{l}$ in three-loop diagrams). Each integration is accompanied by the factor $D_0(2\pi)^{-d}$ with $D_0 = g\nu\mu^{\varepsilon}$, and all ν's will later be canceled out with analogous factors in the energy denominators. As a result, the quantity $I_{12\cdots}^{ab\cdots}$ from Eq. (4.16) is represented as follows:

$$1 \text{ loop}, \quad I_{12\cdots}^{ab\cdots} = [D_0(2\pi)^{-d}] \int d\mathbf{k} N_k \phi_{12\cdots}^{ab\cdots}, \tag{4.37a}$$

$$2 \text{ loops}, \quad I_{12\cdots}^{ab\cdots} = [D_0(2\pi)^{-d}]^2 \int \int d\mathbf{k} d\mathbf{q} N_k N_q \phi_{12\cdots}^{ab\cdots}, \tag{4.37b}$$

$$3 \text{ loops}, \quad I_{12\cdots}^{ab\cdots} = [D_0(2\pi)^{-d}]^3$$
$$\times \int \int \int d\mathbf{k} d\mathbf{q} d\mathbf{l} N_k N_q N_l \phi_{12\cdots}^{ab\cdots}, \tag{4.37c}$$

with N_k from Eq. (1.3). After these scalar factors have been isolated, only the transverse projectors P remain in the vv lines. The nontrivial parts $\phi_{12\cdots}^{ab\cdots}$ of the integrands in Eq. (4.37) are represented as follows:

$$\phi_{12\cdots}^{ab\cdots} = C\phi_E^{-1}\phi_s \bar{I}_{12\cdots}^{ab\cdots}, \tag{4.38}$$

where C is a numerical factor, ϕ_E is the energy denominator, ϕ_s is an additional "scalar factor," which can arise due to contractions over the internal indices, and $\bar{I}_{12\cdots}^{ab\cdots}$ is the nontrivial "index structure" of the integrand, which remains after ϕ_s has been isolated.

Let us explain in more detail the calculation of the factors entering into Eq. (4.38) starting with the energy factors ϕ_E^{-1}. Since the velocity correlation function (1.3) contains the delta function in time, the dots on the rays connected by such correlators have coincident times t. If we assign the time $t = 0$ to the uppermost vertex of a diagram (that is, to the vertex of the composite operator), the independent variables will be the times $t_i < 0$ of the horizontal vv lines. On any of the rays, the times t_i decrease from above to below owing to the retardation property of the functions $\langle\theta\theta'\rangle_0$ in Eq. (2.5). For the normal (not factorizable) one-loop and two-loop diagrams in Fig. 1, the order of the times $t_i < 0$ is determined by the form of the diagram in a unique way, that is, there is only one "temporal version." This is also true for all the three-loop diagrams with two and three rays. However, for two of the three-loop diagrams (Nos. 43, 44 in Fig. 1) there are two equivalent temporal versions (the exchange $t_2 \leftrightarrow t_3$ in diagram No. 43 and $t_1 \leftrightarrow t_2$ in diagram No. 44). This gives the additional factor 2 in the coefficient C in Eq. (4.38) for these two diagrams.

The energy denominator ϕ_E, obtained as the result of the integrations over all time variables, is given by the product of the factors corresponding to the "temporal cross sections" of the diagrams between the horizontal vv lines; to each cross section corresponds the sum of "energies" $\epsilon_{\mathbf{p}} = \nu p^2$ for all intersected $\theta\theta'$ lines. For example, one has

$\phi_E = 2\epsilon_{\mathbf{k}}$ for diagram No. 21 in Fig. 2, $\phi_E = 2\epsilon_{\mathbf{q}}2\epsilon_{\mathbf{k+q}}$ for diagram No. 22, and $\phi_E = 2\epsilon_{\mathbf{q}}[\epsilon_{\mathbf{k}} + \epsilon_{\mathbf{q}} + \epsilon_{\mathbf{k+q}}]$ for diagram No. 31.

The scalar factors ϕ_s in Eq. (4.38) are generated by the vv lines whose vector indices are contracted with the indices of *two* integration momenta in the diagram. This gives rise to expressions of the form $(\mathbf{p}P\mathbf{p}') \equiv p_i P_{ij} p'_j$, where P is the projector that corresponds to the vv line and $\mathbf{p}$, $\mathbf{p}'$ are the momenta contracted to the line (the factors $\pm i$ are not included). In what follows, we denote as $P_{\mathbf{k}}$, $P_{\mathbf{q}}$, and $P_{\mathbf{l}}$ the transverse projectors for the momenta $\mathbf{k}$, $\mathbf{q}$, and $\mathbf{l}$, respectively. Then the scalar factors from the diagrams in Fig. 2 take on the form $\phi_s = (\mathbf{q}P_{\mathbf{k}}\mathbf{q})$ for No. 22 and $\phi_s = 1$ for Nos. 21, 31, because the latter two diagrams do not contain lines vv contracted to two momenta.

The numerical coefficient C in Eq. (4.38) is represented as the product $C = C_1 C_2 C_3$, where C_1 is the symmetry coefficient of the diagram, shown in Fig. 1, $C_2 = \pm 1$ is the sign factor (see Sec. IV A) and $C_3 = 1$ or 2 is the number of the temporal versions. For most of the diagrams one has $C_2 = +1$, but there are two diagrams with $C_2 = -1$ (Nos. 44, 45). The factor C_3 is equal to 1 except for the diagrams Nos. 43, 44 with $C_3 = 2$. In what follows, we shall always present the coefficient C as the product $C = C_1 C_2 C_3$, for example, $C = 1/2 \times 1 \times 1$ for diagrams Nos. 21, 22 in Fig. 2 and $C = 1 \times 1 \times 1$ for diagram No. 31.

Now let us turn to the quantities $\bar{I}_{12\cdots}^{ab\cdots}$ in Eq. (4.38), which remain in the integrands after the scalar factors ϕ_s have been isolated. They have the same stucture for all the diagrams with two and three rays and any number of loops, and two possible structures for the four-ray diagrams, namely,

$$k = 2, \quad \text{n1} = \bar{I}_{12}^{ab} = x_1 x_2 P_{ab};$$

$$k = 3, \quad \text{n2} = \bar{I}_{123}^{abc} = x_1(x+y)_2 y_3 \alpha_a P_{bc};$$

$$k = 4, \quad \text{n3} = \bar{I}_{1234}^{abcd} = x_1 y_2 z_3(x+y+z)_4 \alpha_a \beta_b P_{cd};$$

$$k = 4, \quad \text{n4} = \bar{I}_{1234}^{abcd} = x_1 y_2 z_3(x+y+z)_4 P_{ab}P'_{cd}. \tag{4.39}$$

We have introduced the numbering n1–n4 and in what follows, when describing the diagrams we shall only give the number of the corresponding structure, e.g., $\bar{I} = \text{n1}$ with the specification of the vectors $\mathbf{x}, \mathbf{y}, \mathbf{z}, \boldsymbol{\alpha}, \boldsymbol{\beta}$ and projectors P, P'. In particular, we have $\bar{I} = \text{n1}$ with $\mathbf{x} = \mathbf{k}$, $P = P_{\mathbf{k}}$ for diagram No. 21 in Fig. 2, $\bar{I} = \text{n1}$ with $\mathbf{x} = \mathbf{k+q}$, $P = P_{\mathbf{q}}$ for diagram No. 22, and $\bar{I} = \text{n2}$ with $\mathbf{x} = \mathbf{k}$, $\mathbf{y} = \mathbf{q}$, $\boldsymbol{\alpha} = P_{\mathbf{k}}\mathbf{q}$, $P = P_{\mathbf{q}}$ for diagram No. 31 (quantities like $\boldsymbol{\alpha} = P_{\mathbf{k}}\mathbf{q}$ are undestood as vectors obtained by the action of the matrix $P_{\mathbf{k}}$ onto thevector $\mathbf{q}$).

Our aim is the calculation of the quantities A_i in Eq. (4.20) for each diagram in Fig. 1. They are given by the contractions of the integrals (4.37) with the structures S_i from Eq. (4.19), which leads to the replacement of the factors $\phi_{12\cdots}^{ab\cdots}$ in Eq. (4.37) with the quantities ϕ_i

$=\mathrm{tr}[(S_i)_{1,2,\cdots}^{ab;\cdots}\mathcal{S}\phi_{12\cdots}^{ab;\cdots}]$. Substituting expression (4.38) into this construction gives $\phi_i=C\phi_E^{-1}\phi_s\bar{A}_i$, where

$$\bar{A}_i=\mathrm{tr}[S_i\mathcal{S}\bar{I}] \tag{4.40}$$

are the analogs of quantities (4.20) with the replacement $I\to\bar{I}$. As a result, from the relations (4.20), (4.37), (4.38), and (4.40) one obtains the following explicit formulas for the calculation of the coefficients A_i:

$$1 \text{ loop}, \quad A_i=[D_0(2\pi)^{-d}]\int d\mathbf{k}N_kC\,\phi_E^{-1}\phi_s\bar{A}_i, \tag{4.41a}$$

$$2 \text{ loops}, \quad A_i=[D_0(2\pi)^{-d}]^2\int\int d\mathbf{k}d\mathbf{q}N_kN_qC\,\phi_E^{-1}\phi_s\bar{A}_i, \tag{4.41b}$$

$$3 \text{ loops}, \quad A_i=[D_0(2\pi)^{-d}]^3$$
$$\times\int\int\int d\mathbf{k}d\mathbf{q}d\mathbf{l}N_kN_qN_lC\,\phi_E^{-1}\phi_s\bar{A}_i \tag{4.41c}$$

with $\bar{A}_i$ from Eq. (4.40).

Calculation of these quantities for structures n1 and n2 from Eq. (4.39) and S_i from Eq. (4.19) gives,

$$k=2(\bar{I}=\mathrm{n1}), \quad \bar{A}_1=(\mathbf{x}P\mathbf{x}), \quad \bar{A}_2=(d-1)x^2; \tag{4.42}$$

$$k=3(\bar{I}=\mathrm{n2}), \quad 3\bar{A}_1=(\mathbf{y}\cdot\boldsymbol{\alpha})(\mathbf{x}P\mathbf{x})+(\mathbf{x}\cdot\boldsymbol{\alpha})(\mathbf{y}P\mathbf{y})$$
$$+[(\mathbf{x}+\mathbf{y})\cdot\boldsymbol{\alpha}](\mathbf{x}P\mathbf{y}),$$

$$9\bar{A}_2=[x^2+2(\mathbf{x}\cdot\mathbf{y})][(d-1)(\mathbf{y}\cdot\boldsymbol{\alpha})+2(\mathbf{y}P\boldsymbol{\alpha})]$$
$$+[y^2+2(\mathbf{x}\cdot\mathbf{y})][(d-1)(\mathbf{x}\cdot\boldsymbol{\alpha})+2(\mathbf{x}P\boldsymbol{\alpha})]. \tag{4.43}$$

Analogous expressions can also be obtained for the structures n3 and n4 in Eq. (4.39) for the four-ray diagrams; they are rather cumbersome are will be given later in Sec. VI A.

V. CALCULATION IN THE ONE-LOOP AND TWO-LOOP APPROXIMATIONS

In the one-loop approximation, we need only diagram No. 21 , and in the two-loop approximation, all the four diagrams from Fig. 2 are needed. Using the general rules discussed in the previous section, for the normal diagrams in the notation (4.38), (4.39) we obtain

diagram No. 21, $\quad C=1/2\times1\times1, \quad \phi_s=1, \quad \phi_E=2\epsilon_{\mathbf{k}}$,

$$\bar{I}=\mathrm{n1} \quad\text{with}\quad \mathbf{x}=\mathbf{k}, \quad P=P_{\mathbf{k}} \quad [P\mathbf{x}=0]; \tag{5.1}$$

diagram No. 22, $\quad C=1/2\times1\times1, \quad \phi_s=(\mathbf{q}P_{\mathbf{k}}\mathbf{q})$,

$$\phi_E=4\epsilon_{\mathbf{q}}\epsilon_{\mathbf{k}+\mathbf{q}},$$

$$\bar{I}=\mathrm{n1} \quad\text{with}\quad \mathbf{x}=\mathbf{k}+\mathbf{q}, \quad P=P_{\mathbf{q}}; \tag{5.2}$$

diagram No. 31, $\quad C=1\times1\times1, \quad \phi_s=1$,

$$\phi_E=2\epsilon_{\mathbf{q}}(\epsilon_{\mathbf{k}}+\epsilon_{\mathbf{q}}+\epsilon_{\mathbf{k}+\mathbf{q}}),$$

$$\bar{I}=\mathrm{n2} \quad\text{with}\quad \mathbf{x}=\mathbf{k}, \quad \mathbf{y}=\mathbf{q}, \quad \boldsymbol{\alpha}=P_{\mathbf{k}}\mathbf{q}, \quad P=P_{\mathbf{q}} \quad [(\mathbf{x}\cdot\boldsymbol{\alpha})=0,$$
$$P\mathbf{y}=0]; \tag{5.3}$$

in the square brackets we give simple relations specific of a given set of momenta and projectors, which are useful in the calculations. We also recall that $\epsilon_{\mathbf{p}}=\nu p^2$.

Substituting the explicit expressions (5.1)–(5.3) into the general relations (4.42) and (4.43) gives

diagram No. 21, $\quad \bar{A}_1=0, \quad \bar{A}_2=(d-1)k^2; \tag{5.4}$

diagram No. 22, $\quad \bar{A}_1=(\mathbf{k}P_{\mathbf{q}}\mathbf{k}), \quad \bar{A}_2=(d-1)(\mathbf{k}+\mathbf{q})^2; \tag{5.5}$

diagram No. 31, $\quad 3\bar{A}_1=(\mathbf{q}P_{\mathbf{k}}\mathbf{q})(\mathbf{k}P_{\mathbf{q}}\mathbf{k}),$

$$9\bar{A}_2=(d-1)(\mathbf{q}P_{\mathbf{k}}\mathbf{q})[k^2+2(\mathbf{k}\cdot\mathbf{q})]+2(\mathbf{k}P_{\mathbf{q}}P_{\mathbf{k}}\mathbf{q})[q^2$$
$$+2(\mathbf{k}\cdot\mathbf{q})]. \tag{5.6}$$

A. One-loop approximation

The one-loop approximation $\bar{\Gamma}^{(1)}$ in Eq. (4.6) is determined by only diagram No. 21 in Fig. 2. Substituting the quantities known from Eqs. (5.1) and (5.4) and the relation $\epsilon_{\mathbf{k}}=\nu k^2$ into Eq. (4.41a) gives (we recall that the symmetry coefficient 1/2 is included into C):

diagram No. 21, $\quad A_1=0, \quad A_2=[(d-1)/4]g\mu^\varepsilon U \tag{5.7}$

with the integral $U\equiv(2\pi)^{-d}\int d\mathbf{k}N_k$ from Eq. (2.11). Substituting that expression into Eq. (5.7) gives

diagram No. 21, $\quad A_1=0, \quad A_2=u[(d-1)/4\varepsilon](\mu/m)^\varepsilon,$

$$u=gC_d \tag{5.8}$$

with coefficient C_d from Eq. (2.11)

From the relations (4.23a) and (5.8) we find $B_1=-2\alpha A_2$, $B_2=\alpha(d+1)A_2$ with α from Eq. (4.23a) and A_2 from Eq. (5.8); then from Eqs. (4.35) and (4.36a) we obtain the quantity Γ for diagram: $\Gamma(\text{diagram No. 21})=\alpha A_2[-2n(n-1)+(d+1)\lambda_{nl}]$. Substituting the known expressions for α and A_2 gives

$$\bar{\Gamma}^{(1)}=\bar{\Gamma}(\text{diagram No. 21})$$
$$=u(\mu/m)^\varepsilon\frac{(d+1)\lambda_{nl}-2n(n-1)}{4\varepsilon d(d+2)}. \tag{5.9}$$

Then the relation (4.9a) gives the final result for the $O(u)$ contribution to the renormalization constant,

$$Z_F^{-1} = 1 + [Z_F^{-1}]_1, \quad [Z_F^{-1}]_1 = u \frac{2n(n-1) - (d+1)\lambda_{nl}}{4\varepsilon d(d+2)}. \tag{5.10}$$

B. Two-loop approximation

Consider now the two-loop diagrams Nos. 22, 31 in Fig. 2; the corresponding coefficients $\bar{A}_i$ are known from Eqs. (5.5) and (5.6). They include the quantities $(\mathbf{k}P_\mathbf{q}\mathbf{k}) = k^2\sin^2\vartheta$, $(\mathbf{q}P_\mathbf{k}\mathbf{q}) = q^2\sin^2\vartheta$, $(\mathbf{k}P_\mathbf{q}P_\mathbf{k}\mathbf{q}) = -(\mathbf{k}\cdot\mathbf{q})\sin^2\vartheta$, $(\mathbf{k}\cdot\mathbf{q})^2 = k^2q^2\cos^2\vartheta$, where ϑ is the angle between the vectors $\mathbf{k}$ and $\mathbf{q}$. Substituting these expressions into Eqs. (5.5) and (5.6) gives

diagram No. 22, $\quad \bar{A}_1 = k^2\sin^2\vartheta, \quad \bar{A}_2 = (d-1)(\mathbf{k}+\mathbf{q})^2;$ (5.11)

diagram No. 31, $\quad 3\bar{A}_1 = k^2q^2\sin^4\vartheta,$

$$9\bar{A}_2 = \sin^2\vartheta\{(d-1)q^2[k^2 + 2(\mathbf{k}\cdot\mathbf{q})] - 2(\mathbf{k}\cdot\mathbf{q})$$

$$\times [q^2 + 2(\mathbf{k}\cdot\mathbf{q})]\}$$

$$= q^2\sin^2\vartheta\{(d-1)[k^2 + 2(\mathbf{k}\cdot\mathbf{q})] - 2(\mathbf{k}\cdot\mathbf{q}) - 4k^2\cos^2\vartheta\}. \tag{5.12}$$

Substituting these expressions along with the other needed information from Eqs. (5.2) and (5.3) and the relation $\epsilon_\mathbf{p} = \nu p^2$ into Eq. (4.41b) gives

diagram No. 22, $\quad A_1 = [(g\mu^\varepsilon)^2/8](2\pi)^{-2d}$

$$\times \int \int d\mathbf{k}d\mathbf{q}, N_k N_q \frac{k^2\sin^4\vartheta}{(\mathbf{k}+\mathbf{q})^2},$$

$$A_2 = [(d-1)(g\mu^\varepsilon)^2/8](2\pi)^{-2d}\int\int d\mathbf{k}d\mathbf{q}N_k N_q\sin^2\vartheta; \tag{5.13}$$

diagram No. 31, $\quad 3A_1 = [(g\mu^\varepsilon)^2/4](2\pi)^{-2d}$

$$\times \int\int d\mathbf{k}d\mathbf{q}N_k N_q$$

$$\times \frac{k^2\sin^4\vartheta}{k^2 + q^2 + (\mathbf{k}\cdot\mathbf{q})},$$

$$9A_2 = [(g\mu^\varepsilon)^2/4](2\pi)^{-2d}\int\int d\mathbf{k}d\mathbf{q}N_k N_q$$

$$\times \frac{\sin^2\vartheta\{(d-1)[k^2 + 2(\mathbf{k}\cdot\mathbf{q})] - 2(\mathbf{k}\cdot\mathbf{q}) - 4k^2\cos^2\vartheta\}}{k^2 + q^2 + (\mathbf{k}\cdot\mathbf{q})}. \tag{5.14}$$

We note that in the coefficients $A_{1,2}$ for diagram No. 31, the factor q^2 from $\epsilon_\mathbf{q}$ in the denominators cancels out with the analogous factor in the numerators, while in the coefficient A_2 for diagram No. 22, a similar cancellation of the factor $(\mathbf{k}+\mathbf{q})^2$ takes place.

The denominators in the integrals (5.13) and (5.14) are symmetrical with respect to the permutation $\mathbf{k}\leftrightarrow\mathbf{q}$. This allows one to perform the analogous symmetrization in the numerators, which is equivalent to the replacement $k^2 \to (k^2 + q^2)/2$ in the latter. Then the expressions simplify and reduce to linear combinations of the following standard integrals:

$$H_{2p} = (2\pi)^{-2d}\int\int d\mathbf{k}d\mathbf{q}N_k N_q\sin^{2p}\vartheta, \quad p=1,2, \tag{5.15}$$

$$h = (2\pi)^{-2d}\int\int d\mathbf{k}d\mathbf{q}N_k N_q(\mathbf{k}\cdot\mathbf{q})\sin^4\vartheta/(\mathbf{k}+\mathbf{q})^2, \tag{5.16}$$

$$h_{2p} = (2\pi)^{-2d}\int\int d\mathbf{k}d\mathbf{q}N_k N_q(\mathbf{k}\cdot\mathbf{q})\sin^{2p}\vartheta/[k^2 + q^2$$

$$+ (\mathbf{k}\cdot\mathbf{q})], \quad p=1,2. \tag{5.17}$$

The coefficients A_i in Eqs. (5.13) and (5.14) are expressed in terms of these integrals as follows:

diagram No. 22, $\quad A_1 = [(g\mu^\varepsilon)^2/8][H_4/2 - h],$

$$A_2 = [(g\mu^\varepsilon)^2/8][(d-1)H_2]; \tag{5.18}$$

diagram No. 31, $\quad 3A_1 = [(g\mu^\varepsilon)^2/4][H_4/2 - h_4/2],$

$$9A_2 = [(g\mu^\varepsilon)^2/4][(d-5)H_2/2 + 2H_4 + 3(d-1)h_2/2 - 2h_4]. \tag{5.19}$$

These expressions along with Eq. (4.23a) for diagram No. 22 and Eq. (4.23b) for diagram No. 31 give the coefficients B_i, then using Eqs. (4.35), (4.36a), and (4.36b) one obtains the corresponding quantities $\bar{\Gamma}$(diagram No. 22) and $\bar{\Gamma}$(diagram No. 31); the answers are represented as linear combinations of the standard integrals (5.15)–(5.17).

The two-loop quantity $\bar{\Gamma}^{(2)}$ also includes the contribution from the factorizable diagram No. 41 with the symmetry coefficient 1/8; see Fig. 1. It reduces to the contraction of the vertex factor V_{1234} with the product $T_{12}T_{34}$ of two identical one-loop blocks similar to diagram No. 21. In the notation of Eqs. (4.24)–(4.28) this contribution has the form

$$\Gamma = C V_{1234}[B_1 w_1 w_2 + B_2 w^2\delta_{12}][B_1 w_3 w_4 + B_2 w^2\delta_{34}] \equiv F\bar{\Gamma}, \tag{5.20}$$

where $B_{1,2}$ are the known coefficients for the one-loop diagram No. 21 (see Sec. V A) and C is an additional symmetry coefficient; in the case at hand, $C=1/2$. Let us explain its origin. By definition, the quantities $B_{1,2}$ for diagram No. 21 already include its symmetry coefficient 1/2 [in the factor C in Eq. (4.38)], which gives 1/4 for the product of two such blocks. Therefore, in order to obtain the correct symmetry coefficient 1/8 for diagram No. 41, the additional coefficient $C=1/2$ should be included.

Multiplying the expressions in the square brackets in Eq. (5.20) and taking into account the definition of the coefficients k_i in Eq. (4.36) gives

$$\bar{\Gamma}(\text{diagram No. 41}) = [1/2][k_1 B_1^2 + 2k_2 B_1 B_2 + k_3 B_2^2] \tag{5.21}$$

with coefficients $k_{1,2,3}$ from Eq. (4.36c) and known quantities $B_{1,2}$ for the one-loop diagram No. 21. In what follows, the same scheme will be used for the calculation of the contributions of the three-loop factorizable diagrams Nos. 46, 51, 61; the coefficients k_i from Eqs. (4.36d) and (4.36e) will be involved.

We have found all terms in the two-loop expression

$$\bar{\Gamma}^{(2)} = \bar{\Gamma}(\text{diagram No. 22}) + \bar{\Gamma}(\text{diagram No. 31})$$

$$+ \bar{\Gamma}(\text{diagram No. 41}). \tag{5.22}$$

Now Eq. (4.9b) is used to determine the two-loop contribution $[Z_F^{-1}]_2$ in the renormalization constant Z_F^{-1}, with $\bar{\Gamma}^{(1)}$ from Eq. (5.9), $\bar{\Gamma}^{(2)}$ from Eq. (5.22), and $[Z_F^{-1}]_1$ from Eq. (5.10). It is also necessary to set $\mu = m$ in all the diagrams of $\bar{\Gamma}^{(1,2)}$ in order to eliminate contributions with the logarithms $\ln(\mu/m)$ (they would be canceled with the contributions of the diagrams with self-energy insertions, which we already omitted).

All the quantities in Eq. (4.9b) are known explicitly, except for the contributions of diagrams Nos. 22, 31, for which we only know the expressions of the coefficients A_i in terms of the standard integrals (5.15)–(5.17). In order to calculate the quantity (4.9b), we need only their divergent parts $\sim 1/\varepsilon^2$ and $1/\varepsilon$, but for the three-loop calculation we shall also need the zero order in ε (constant) terms.

Calculation of these standard integrals is a separate task and will be discussed in the next section.

C. Calculation of the two-loop integrals Eqs. (5.15)–(5.17)

In this section we denote $\mathbf{n}_k \equiv \mathbf{k}/k$ for any vector $\mathbf{k}$, $d\mathbf{n}_k$ is the area element of the unit d-dimensional sphere and $\langle \cdots \rangle$ is the averaging over the sphere. In particular,

$$\int d\mathbf{k} N_k \cdots = \int_m^\infty \frac{dk}{k^{1+\varepsilon}} \int d\mathbf{n}_k \cdots = S_d \int_m^\infty \frac{dk}{k^{1+\varepsilon}} \langle \cdots \rangle \tag{5.23}$$

with N_k from Eq. (1.3); $S_d = 2\pi^{d/2}/\Gamma(d/2)$ is the surface area of the unit sphere.

For any two vectors with the angle ϑ between them, the following formulas will be useful:

$$\alpha_{2n} \equiv \langle \cos^{2n} \vartheta \rangle = \frac{(2n-1)!!}{d(d+2) \cdots (d+2n-2)} \tag{5.24}$$

with $n = 1, 2, \ldots$ (obviously, $\alpha_0 \equiv \langle 1 \rangle = 1$). From Eq. (5.24) one easily obtains

$$\langle \sin^2 \vartheta \cos^{2n} \vartheta \rangle = \frac{(d-1)}{(d+2n)} \alpha_{2n}, \quad \langle \sin^4 \vartheta \cos^{2n} \vartheta \rangle$$

$$= \frac{(d^2-1)}{(d+2n)(d+2n+2)} \alpha_{2n} \tag{5.25}$$

with $n = 0, 1, 2, \ldots$ and α_{2n} from Eq. (5.24).

In the notation introduced above, the integrals H_{2p} in Eq. (5.15) are written in the form

$$H_{2p} = C_d^2 \int_m^\infty \frac{dk}{k^{1+\varepsilon}} \int_m^\infty \frac{dq}{q^{1+\varepsilon}} \langle \sin^{2p} \vartheta \rangle, \quad p = 1, 2. \tag{5.26}$$

Then Eq. (5.25) gives

$$H_2 = C_d^2 \frac{m^{-2\varepsilon}(d-1)}{d\varepsilon^2}, \quad H_4 = C_d^2 \frac{m^{-2\varepsilon}(d^2-1)}{d(d+2)\varepsilon^2}. \tag{5.27}$$

Now let us turn to the integrals h_{2p} in Eq. (5.17). Expanding their integrands in $(\mathbf{k} \cdot \mathbf{q})$ gives

$$h_{2p} = C_d^2 \sum_{l=0}^\infty (-1)^l \int_m^\infty \frac{dk}{k^{1+\varepsilon}} \int_m^\infty \frac{dq}{q^{1+\varepsilon}} \left(\frac{kq}{k^2+q^2} \right)^{l+1}$$

$$\times \langle \sin^{2p} \vartheta \cos^{l+1} \vartheta \rangle. \tag{5.28}$$

The average $\langle \sin^{2p} \vartheta \cos^{l+1} \vartheta \rangle$ differs from zero only for odd l, and the series in Eq. (5.28) can be written as

$$h_{2p} = -C_d^2 \sum_{n=0}^\infty I_n(m) \langle \sin^{2p} \vartheta \cos^{2n+2} \vartheta \rangle \tag{5.29}$$

with the integral

$$I_n(m) \equiv \int_m^\infty \frac{dk}{k^{1+\varepsilon}} \int_m^\infty \frac{dq}{q^{1+\varepsilon}} \left(\frac{kq}{k^2+q^2} \right)^{2n+2} = m^{-2\varepsilon} I_n(1). \tag{5.30}$$

Using the identity

$$I_n(m) = -\frac{1}{2\varepsilon} \mathcal{D}_m I_n(m), \quad \mathcal{D}_m \equiv m \partial/\partial m, \tag{5.31}$$

which follows from the last equality in Eq. (5.30), the integral $I_n(m)$ can be represented in the form

$$I_n(m) = \frac{m^{-2\varepsilon}}{\varepsilon} \int_1^\infty \frac{dk}{k^{1+\varepsilon}} \left(\frac{k}{k^2+1} \right)^{2n+2}, \tag{5.32}$$

where the number of integrations is reduced and the pole in ε is isolated explicitly. Expanding the integrand in Eq. (5.32) in ε and neglecting the terms of order $O(\varepsilon)$ and higher with the desired accuracy we obtain

$$I_n(m) \simeq m^{-2\varepsilon} \int_1^\infty \frac{dk\, k^{2n+1}}{(k^2+1)^{2n+2}} (\varepsilon^{-1} - \ln k)$$

$$= m^{-2\varepsilon} \frac{(n!)^2}{4(2n+1)!} (\varepsilon^{-1} - \mathcal{B}_n), \tag{5.33}$$

where the quantities $\mathcal{B}_n$, needed only for the three-loop calculation, can be represented as finite sums,

$$\mathcal{B}_n = \ln 2 + \frac{(2n+1)!}{n!} \sum_{k=0}^n \frac{(-1)^k[(1/2)^{n+k}-1]}{k!(n-k)!(n+k+1)^2}. \tag{5.34}$$

For the integrals h_{2p} in Eq. (5.17) this gives

$$h_2 = m^{-2\varepsilon} C_d^2 (d-1) \sum_{n=0}^\infty \frac{n!\, 2^{-n-2}}{d(d+2)\cdots(d+2n+2)}$$

$$\times (-\varepsilon^{-1} + \mathcal{B}_n); \tag{5.35a}$$

$$h_4 = m^{-2\varepsilon} C_d^2 (d^2-1) \sum_{n=0}^\infty \frac{n!\, 2^{-n-2}}{d(d+2)\cdots(d+2n+4)}$$

$$\times (-\varepsilon^{-1} + \mathcal{B}_n). \tag{5.35b}$$

Expanding the integrand in Eq. (5.16) in $2(\mathbf{k}\cdot\mathbf{q})$ and proceeding as above for h_{2p}, we obtain an analogous expression for the integral h,

$$h = m^{-2\varepsilon} C_d^2 (d^2-1) \sum_{n=0}^\infty \frac{n!\, 2^{n-1}}{d(d+2)\cdots(d+2n+4)}$$

$$\times (-\varepsilon^{-1} + \mathcal{B}_n). \tag{5.35c}$$

The $O(\varepsilon^{-1})$ terms in Eqs. (5.35) can be expressed in terms of the hypergeometric series (see, e.g., [27])

$$F(a,b;c;z) \equiv 1 + \frac{ab}{c} z + \frac{a(a+1)b(b+1)}{c(c+1)} \frac{z^2}{2!} + \cdots \tag{5.36}$$

as follows:

$$h_2 = \frac{m^{-2\varepsilon} C_d^2(d-1)}{4d(d+2)} [-\varepsilon^{-1} F(1,1;d/2+2;1/4)$$

$$+ (d+2)\mathcal{C}_2(d)], \tag{5.37a}$$

$$h_4 = \frac{m^{-2\varepsilon} C_d^2(d^2-1)}{4d(d+2)(d+4)} [-\varepsilon^{-1} F(1,1;d/2+3;1/4)$$

$$+ (d+4)\mathcal{C}_4(d)], \tag{5.37b}$$

$$h = \frac{m^{-2\varepsilon} C_d^2(d^2-1)}{2d(d+2)(d+4)} [-\varepsilon^{-1} F(1,1;d/2+3;1)$$

$$+ (d+4)\mathcal{C}(d)], \tag{5.37c}$$

and for the $O(1)$ terms one has

$$\mathcal{C}_2(d) = \sum_{n=0}^\infty \frac{n!\mathcal{B}_n}{4^n(d/2+1)\cdots(d/2+1+n)}, \tag{5.38a}$$

$$\mathcal{C}_4(d) = \sum_{n=0}^\infty \frac{n!\mathcal{B}_n}{4^n(d/2+2)\cdots(d/2+2+n)} = \mathcal{C}_2(d+2), \tag{5.38b}$$

$$\mathcal{C}(d) = \sum_{n=0}^\infty \frac{n!\mathcal{B}_n}{(d/2+2)\cdots(d/2+2+n)}. \tag{5.38c}$$

It is worth noting that the series entering into Eqs. (5.37) and (5.38) are convergent; this fact is nontrivial for h since $|z| = 1$ is the convergence radius for the corresponding series.

For $F(\cdots)$ in Eq. (5.37c) one has $F(1,1;d/2+3;1) = (d+4)/(d+2)$ for any d, while the expressions for $F(\cdots)$ in Eqs. (5.37a) and (5.37b) simplify only for integer d; see [27]. In particular, for $d=2$ and $d=3$ one has

$$d=2, \quad F(1,1;d/2+2;1/4) = 8[-3\ln(4/3)+1] \simeq 1.0956,$$

$$F(1,1;d/2+3;1/4) = 6[18\ln(4/3)-5] \simeq 1.0696,$$

$$\mathcal{C}_2 \simeq 0.3671, \quad \mathcal{C}_4 \simeq 0.2411, \quad \mathcal{C} \simeq 0.2917; \tag{5.39a}$$

$$d=3, \quad F(1,1;d/2+2;1/4) = 10(\pi\sqrt{3}-16/3) \simeq 1.0806,$$

$$F(1,1;d/2+3;1/4) = 14(-15\pi\sqrt{3}+82)/5 \simeq 1.0613,$$

$$\mathcal{C}_2 \simeq 0.2912, \quad \mathcal{C}_4 \simeq 0.2056, \quad \mathcal{C} \simeq 0.2412; \tag{5.39b}$$

and for the other integer d analogous expressions can be obtained from the recurrent relation

$$3F(1,1;d/2+2;1/4)+(d+2)F(1,1;d/2+3;1/4)/(d+4)=4 \tag{5.40}$$

valid for all d. In Eq. (5.39) we also included the numerical values for the coefficients $\mathcal{C}_{2,4}$ and $\mathcal{C}$ obtained from the series (5.38).

Substituting all these expressions for the integrals into Eqs. (5.18) and (5.19) gives the final answers for the coefficients A_i of the diagrams Nos. 22, 31,

$$\text{diagram No. 22,} \quad A_1 = \frac{u^2(\mu/m)^{2\varepsilon}(d^2-1)}{16d(d+2)}$$

$$\times \left[\frac{1}{\varepsilon^2} + \frac{1}{(d+2)\varepsilon} - \frac{1}{2}\mathcal{C}(d) \right],$$

$$A_2 = \frac{u^2(\mu/m)^{2\varepsilon}(d-1)^2}{16d\varepsilon^2}; \tag{5.41}$$

$$\text{diagram No. 31,} \quad A_1 = \frac{u^2(\mu/m)^{2\varepsilon}}{24d(d+2)} \left[\frac{1}{\varepsilon^2} + \frac{F(1,1;d/2+3;1/4)}{4(d+4)\varepsilon} \right.$$

$$\left. - \frac{1}{8}\mathcal{C}_4(d) \right],$$

$$A_2 = \frac{u^2(\mu/m)^{2\varepsilon}(d-1)}{24d(d+2)}\left[\frac{(d-2)(d+3)}{3\varepsilon^2}\right.$$

$$-\frac{(d-1)F(1,1;d/2+2;1/4)}{4\varepsilon}$$

$$+\frac{(d+1)F(1,1;d/2+3;1/4)}{3(d+4)\varepsilon}+\frac{1}{8}(d-1)(d+2)\mathcal{C}_2(d)$$

$$\left.-\frac{1}{6}(d+1)\mathcal{C}_4(d)\right] \tag{5.42}$$

with $F(\cdots)$ from Eq. (5.36) and $\mathcal{C},\mathcal{C}_{2,4}$ from Eq. (5.38). From these expressions, using the standard general scheme, one obtains the contributions of the diagrams Nos. 22, 31 into Eq. (5.22) and then the two-loop contribution $[Z_F^{-1}]_2$ into the renormalization constant Z_F^{-1}, presented earlier in Ref. [10].

VI. THREE-LOOP APPROXIMATION
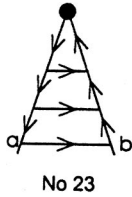
A. Scalarization of the three-loop diagrams

All the needed three-loop diagrams with the symmetry coefficients are given in Fig. 1. Below we shall describe them in more detail and give in a compact form the complete set of relations that allow one to express the coefficients A_i in Eq. (4.20) for any given diagram in terms of the scalar integrals (4.41c). We recall that all the external momenta in the diagrams are set equal to zero.

We begin with the normal (not factorizable) diagrams. For these, the integration momenta **k**, **q**, **l** are always assigned to the horizontal lines $\langle vv \rangle$ in the following order: **k** flows via the uppermost line, **q** flows via the middle line, and **l** flows via the lowest line. Then in order to determine the momenta for all lines in the diagram, it is sufficient to show (by an arrow) the chosen direction of the momentum in each line. The needed derivatives ∂ on the lines are always implied (for the one-loop and two-loop diagrams, they were shown explicitly by dots in Fig. 2). The numerical indices $1,2,\ldots$ of the upper dots are always chosen to increase from the left to the right [like in Eq. (4.17) and in the diagrams in Fig. 2]; the positions of the letter indices $a,b,\ldots$ in the diagram are always shown explicitly. This information allows one to completely restore the configuration of the momenta and the form of the index structures (4.39) for any diagram.

Now we turn to the description of specific diagrams in this notation. For any diagram, we give the directions of the momenta, positions of the indices $a,b,\ldots$, and forms of all cofactors in Eq. (4.38) in the same form as in Eqs. (5.1)–(5.3):
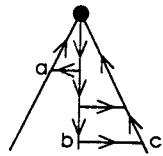
The two-ray diagram No. 23,

No 23

$$C = 1/2 \times 1 \times 1, \quad \phi_s = (\mathbf{l}P_{\mathbf{q}}\mathbf{l})\big[(\mathbf{q}+\mathbf{l})P_{\mathbf{k}}(\mathbf{q}+\mathbf{l})\big],$$
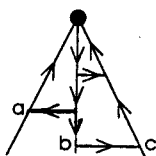
$$\phi_E = 8\epsilon_{\mathbf{l}}\epsilon_{\mathbf{q}+\mathbf{l}}\epsilon_{\mathbf{k}+\mathbf{q}+\mathbf{l}},$$

$$\bar{I} = n1 \quad \text{with} \quad \mathbf{x} = \mathbf{k}+\mathbf{q}+\mathbf{l}, \; P = P_{\mathbf{l}}. \tag{6.1}$$
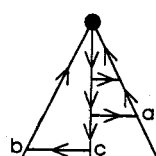
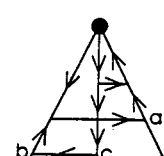The three-ray normal diagrams,

No 32   No 33   No 34   No 35

$$(6.2)$$

For these, one has

$$\text{diagram No. 32,} \quad C = 1 \times 1 \times 1, \quad \phi_s = (\mathbf{l}P_{\mathbf{q}}\mathbf{l}),$$

$$\phi_E = 4\,\epsilon_{\mathbf{l}}\epsilon_{\mathbf{q}+\mathbf{l}}(\epsilon_{\mathbf{k}}+\epsilon_{\mathbf{q}+\mathbf{l}}+\epsilon_{\mathbf{k}+\mathbf{q}+\mathbf{l}}),$$

$$\bar{I} = n2 \quad \text{with} \quad \mathbf{x} = \mathbf{k}, \mathbf{y} = \mathbf{q}+\mathbf{l}, \quad \boldsymbol{\alpha} = P_{\mathbf{k}}(\mathbf{q}+\mathbf{l}),$$

$$P = P_{\mathbf{l}} \; [(\mathbf{x}\cdot\boldsymbol{\alpha})=0]; \tag{6.3}$$

diagram No. 33, $C = 1 \times 1 \times 1$, $\phi_s = [\mathbf{l}P_{\mathbf{k}}(\mathbf{q}+\mathbf{l})]$,

$$\phi_E = 2\epsilon_{\mathbf{l}}(\epsilon_{\mathbf{q}} + \epsilon_{\mathbf{l}} + \epsilon_{\mathbf{q}+\mathbf{l}})(\epsilon_{\mathbf{q}} + \epsilon_{\mathbf{k}+\mathbf{l}} + \epsilon_{\mathbf{k}+\mathbf{q}+\mathbf{l}}),$$

$\bar{I} = $ n2 with $\mathbf{x} = \mathbf{q}$, $\mathbf{y} = \mathbf{k}+\mathbf{l}$, $\boldsymbol{\alpha} = P_{\mathbf{q}}\mathbf{l}$,

$$P = P_{\mathbf{l}} \quad [(\mathbf{x} \cdot \boldsymbol{\alpha}) = 0]; \qquad (6.4)$$

diagram No. 34, $C = 1 \times 1 \times 1$, $\phi_s = [\mathbf{q}P_{\mathbf{k}}(\mathbf{q}+\mathbf{l})]$,

$$\phi_E = 2\epsilon_{\mathbf{l}}(\epsilon_{\mathbf{q}} + \epsilon_{\mathbf{l}} + \epsilon_{\mathbf{q}+\mathbf{l}})(\epsilon_{\mathbf{l}} + \epsilon_{\mathbf{k}+\mathbf{q}} + \epsilon_{\mathbf{k}+\mathbf{q}+\mathbf{l}}),$$

$\bar{I} = $ n2 with $\mathbf{x} = \mathbf{l}$, $\mathbf{y} = \mathbf{k}+\mathbf{q}$, $\boldsymbol{\alpha} = P_{\mathbf{q}}\mathbf{l}$,

$$P = P_{\mathbf{l}} \quad [P\mathbf{x} = 0]; \qquad (6.5)$$

diagram No. 35, $C = 1 \times 1 \times 1$, $\phi_s = (\mathbf{q}P_{\mathbf{k}}\mathbf{l})$,

$$\phi_E = 2\epsilon_{\mathbf{l}}(\epsilon_{\mathbf{q}} + \epsilon_{\mathbf{l}} + \epsilon_{\mathbf{q}-\mathbf{l}})(\epsilon_{\mathbf{k}+\mathbf{q}} + \epsilon_{\mathbf{k}+\mathbf{l}} + \epsilon_{\mathbf{q}-\mathbf{l}}),$$

$\bar{I} = $ n2 with $\mathbf{x} = \mathbf{k}+\mathbf{l}$, $\mathbf{y} = \mathbf{q}-\mathbf{l}$, $\boldsymbol{\alpha} = P_{\mathbf{q}}\mathbf{l}$, $P = P_{\mathbf{l}}$.
(6.6)

The structure $\bar{I} = $ n2 from Eq. (4.39) is the same for all these diagrams; the corresponding quantities $\bar{A}_i$ are determined by the general formula (4.43) in which the specific values of the vectors $\mathbf{x}, \mathbf{y}, \mathbf{z}, \boldsymbol{\alpha}$ and projectors P for any given diagram should be substituted from Eqs. (6.3)–(6.6):

The four-ray normal diagrams,

No 42   No 43   No 44   No 45   (6.7)
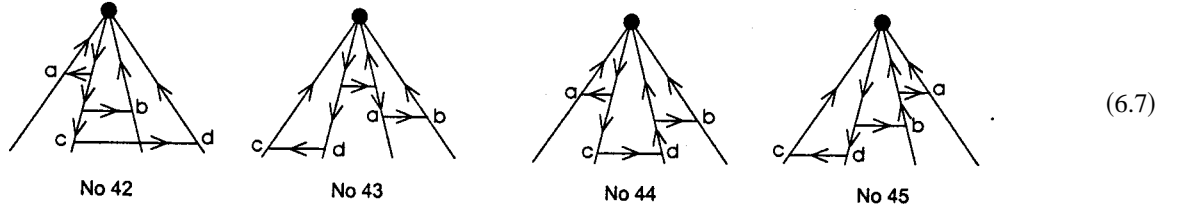
For these, one has,

diagram No. 42, $C = 1 \times 1 \times 1$, $\phi_s = 1$,

$$\phi_E = 2\epsilon_{\mathbf{l}}(\epsilon_{\mathbf{q}} + \epsilon_{\mathbf{l}} + \epsilon_{\mathbf{q}+\mathbf{l}})(\epsilon_{\mathbf{k}} + \epsilon_{\mathbf{q}} + \epsilon_{\mathbf{l}} + \epsilon_{\mathbf{k}+\mathbf{q}+\mathbf{l}}),$$

$\bar{I} = $ n3 with $\mathbf{x} = \mathbf{k}$, $\mathbf{y} = \mathbf{q}$, $\mathbf{z} = \mathbf{l}$, $\boldsymbol{\alpha} = P_{\mathbf{k}}(\mathbf{q}+\mathbf{l})$,

$$\boldsymbol{\beta} = P_{\mathbf{q}}\mathbf{l}, \quad P = P_{\mathbf{l}}$$

$$[(\mathbf{x} \cdot \boldsymbol{\alpha}) = 0, (\mathbf{y} \cdot \boldsymbol{\beta}) = 0, P\mathbf{z} = 0]; \qquad (6.8)$$

diagram No. 43, $C = 1/2 \times 1 \times 2$, $\phi_s = (\mathbf{q}P_{\mathbf{k}}\mathbf{l})$,

$$\phi_E = 4\epsilon_{\mathbf{l}}(\epsilon_{\mathbf{q}} + \epsilon_{\mathbf{l}})(\epsilon_{\mathbf{q}} + \epsilon_{\mathbf{l}} + \epsilon_{\mathbf{k}-\mathbf{q}} + \epsilon_{\mathbf{k}+\mathbf{l}}),$$

$\bar{I} = $ n4 with $\mathbf{x} = \mathbf{q}$, $\mathbf{y} = \mathbf{l}$, $\mathbf{z} = \mathbf{k}-\mathbf{q}$, $P = P_{\mathbf{l}}$,

$$P' = P_{\mathbf{q}}$$

$$[P\mathbf{y} = 0, P'\mathbf{x} = 0]; \qquad (6.9)$$

diagram No. 44, $C = 1/2 \times (-1) \times 2$, $\phi_s = 1$,

$$\phi_E = 2\epsilon_{\mathbf{l}}(\epsilon_{\mathbf{q}} + \epsilon_{\mathbf{l}} + \epsilon_{\mathbf{l}-\mathbf{q}})(\epsilon_{\mathbf{k}} + \epsilon_{\mathbf{q}} + \epsilon_{\mathbf{k}+\mathbf{l}} + \epsilon_{\mathbf{l}-\mathbf{q}}),$$

$\bar{I} = $ n3 with $\mathbf{x} = \mathbf{k}$, $\mathbf{y} = \mathbf{q}$, $\mathbf{z} = \mathbf{l}-\mathbf{q}$, $\boldsymbol{\alpha} = P_{\mathbf{k}}\mathbf{l}$, $\boldsymbol{\beta} = P_{\mathbf{q}}\mathbf{l}$,

$$P = P_{\mathbf{l}}$$

$$[(\mathbf{x} \cdot \boldsymbol{\alpha}) = 0, \ (\mathbf{y} \cdot \boldsymbol{\beta}) = 0, \ P(\mathbf{y}+\mathbf{z}) = 0]; \qquad (6.10)$$

diagram No. 45, $C = 1 \times (-1) \times 1$, $\phi_s = 1$,

$$\phi_E = 2\epsilon_{\mathbf{l}}(\epsilon_{\mathbf{q}} + \epsilon_{\mathbf{l}} + \epsilon_{\mathbf{q}+\mathbf{l}})(\epsilon_{\mathbf{k}} + \epsilon_{\mathbf{l}} + \epsilon_{\mathbf{q}-\mathbf{k}} + \epsilon_{\mathbf{q}+\mathbf{l}}),$$

$\bar{I} = $ n3 with $\mathbf{x} = \mathbf{k}$, $\mathbf{y} = \mathbf{l}$, $\mathbf{z} = \mathbf{q}-\mathbf{k}$, $\boldsymbol{\alpha} = P_{\mathbf{k}}\mathbf{q}$,

$$\boldsymbol{\beta} = P_{\mathbf{q}}\mathbf{l}, \quad P = P_{\mathbf{l}}$$

$$[(\mathbf{x} \cdot \boldsymbol{\alpha}) = 0, \ \{(\mathbf{x}+\mathbf{z}) \cdot \boldsymbol{\beta}\} = 0, P\mathbf{y} = 0]. \qquad (6.11)$$

Three diagrams have the index structure $\bar{I} = $ n3 from Eq. (4.39) and one diagram has the structure $\bar{I} = $ n4; $(\mathbf{x} \cdot \boldsymbol{\alpha}) = 0$ for all the diagrams with $\bar{I} = $ n3.

Below we give the expressions for the coefficients $\bar{A}_i$ for the structures $\bar{I} = $ n3,n4, analogous to Eqs. (4.42) and (4.43).

For $\bar{I}=$n3 from Eqs. (4.39) and (4.40) using the relation $(\mathbf{x}\cdot\boldsymbol{\alpha})=0$ one obtains

$$12\bar{A}_1=(\mathbf{x}P\mathbf{x})[(\mathbf{y}\cdot\boldsymbol{\alpha})(\mathbf{z}\cdot\boldsymbol{\beta})+(\mathbf{y}\cdot\boldsymbol{\beta})(\mathbf{z}\cdot\boldsymbol{\alpha})]+(\mathbf{y}P\mathbf{y})(\mathbf{z}\cdot\boldsymbol{\alpha})(\mathbf{x}\cdot\boldsymbol{\beta})+(\mathbf{z}P\mathbf{z})(\mathbf{x}\cdot\boldsymbol{\beta})(\mathbf{y}\cdot\boldsymbol{\alpha})+2(\mathbf{x}P\mathbf{y})[(\mathbf{y}\cdot\boldsymbol{\alpha})(\mathbf{z}\cdot\boldsymbol{\beta})+(\mathbf{z}\cdot\boldsymbol{\alpha})\{(\mathbf{x}+\mathbf{y}$$
$$+\mathbf{z})\cdot\boldsymbol{\beta}\}]+2(\mathbf{x}P\mathbf{z})[(\mathbf{y}\cdot\boldsymbol{\beta})(\mathbf{z}\cdot\boldsymbol{\alpha})+(\mathbf{y}\cdot\boldsymbol{\alpha})\{(\mathbf{x}+\mathbf{y}+\mathbf{z})\cdot\boldsymbol{\beta}\}]+2(\mathbf{y}P\mathbf{z})(\mathbf{x}\cdot\boldsymbol{\beta})[(\mathbf{z}+\mathbf{y})\cdot\boldsymbol{\alpha}];$$

$$72\bar{A}_2=U_1\{(d-1)[(\mathbf{y}\cdot\boldsymbol{\alpha})(\mathbf{z}\cdot\boldsymbol{\beta})+(\mathbf{y}\cdot\boldsymbol{\beta})(\mathbf{z}\cdot\boldsymbol{\alpha})]+2(\mathbf{y}P\boldsymbol{\alpha})(\mathbf{z}\cdot\boldsymbol{\beta})+2(\mathbf{z}P\boldsymbol{\alpha})(\mathbf{y}\cdot\boldsymbol{\beta})+2(\mathbf{y}P\boldsymbol{\beta})(\mathbf{z}\cdot\boldsymbol{\alpha})+2(\mathbf{z}P\boldsymbol{\beta})(\mathbf{y}\cdot\boldsymbol{\alpha})$$
$$+2(\mathbf{y}P\mathbf{z})(\boldsymbol{\alpha}\cdot\boldsymbol{\beta})\}+U_2\{(d-1)(\mathbf{z}\cdot\boldsymbol{\alpha})(\mathbf{x}\cdot\boldsymbol{\beta})+2(\mathbf{x}P\boldsymbol{\alpha})(\mathbf{z}\cdot\boldsymbol{\beta})+2(\mathbf{z}P\boldsymbol{\alpha})(\mathbf{x}\cdot\boldsymbol{\beta})+2(\mathbf{x}P\boldsymbol{\beta})(\mathbf{z}\cdot\boldsymbol{\alpha})+2(\mathbf{x}P\mathbf{z})(\boldsymbol{\alpha}\cdot\boldsymbol{\beta})\}$$
$$+U_3\{(d-1)(\mathbf{y}\cdot\boldsymbol{\alpha})(\mathbf{x}\cdot\boldsymbol{\beta})+2(\mathbf{x}P\boldsymbol{\alpha})(\mathbf{y}\cdot\boldsymbol{\beta})+2(\mathbf{y}P\boldsymbol{\alpha})(\mathbf{x}\cdot\boldsymbol{\beta})+2(\mathbf{x}P\boldsymbol{\beta})(\mathbf{y}\cdot\boldsymbol{\alpha})+2(\mathbf{x}P\mathbf{y})(\boldsymbol{\alpha}\cdot\boldsymbol{\beta})\}+2(d-1)[(\mathbf{z}\cdot\boldsymbol{\alpha})$$
$$\times(\mathbf{z}\cdot\boldsymbol{\beta})(\mathbf{x}\cdot\mathbf{y})+(\mathbf{y}\cdot\boldsymbol{\alpha})(\mathbf{y}\cdot\boldsymbol{\beta})(\mathbf{x}\cdot\mathbf{z})]+2[(\mathbf{z}P\boldsymbol{\alpha})(\mathbf{z}\cdot\boldsymbol{\beta})(\mathbf{x}\cdot\mathbf{y})+(\mathbf{y}P\boldsymbol{\alpha})(\mathbf{y}\cdot\boldsymbol{\beta})(\mathbf{x}\cdot\mathbf{z})+(\mathbf{x}P\boldsymbol{\alpha})(\mathbf{x}\cdot\boldsymbol{\beta})(\mathbf{y}\cdot\mathbf{z})+(\mathbf{z}P\boldsymbol{\beta})(\mathbf{z}\cdot\boldsymbol{\alpha})$$
$$\times(\mathbf{x}\cdot\mathbf{y})+(\mathbf{y}P\boldsymbol{\beta})(\mathbf{y}\cdot\boldsymbol{\alpha})(\mathbf{x}\cdot\mathbf{z})]+2(\boldsymbol{\alpha}\cdot\boldsymbol{\beta})[(\mathbf{x}P\mathbf{x})(\mathbf{y}\cdot\mathbf{z})+(\mathbf{y}P\mathbf{y})(\mathbf{x}\cdot\mathbf{z})+(\mathbf{z}P\mathbf{z})(\mathbf{x}\cdot\mathbf{y})];$$

$$9\bar{A}_3=U_4\{(d-1)(\boldsymbol{\alpha}\cdot\boldsymbol{\beta})+2(\boldsymbol{\alpha}P\boldsymbol{\beta})\}. \tag{6.12}$$

Here and below in Eq. (6.14)

$$U_1\equiv x^2+2(\mathbf{x}\cdot\mathbf{y})+2(\mathbf{x}\cdot\mathbf{z}),\quad U_2\equiv y^2+2(\mathbf{x}\cdot\mathbf{y})+2(\mathbf{y}\cdot\mathbf{z}),$$

$$U_3\equiv z^2+2(\mathbf{x}\cdot\mathbf{z})+2(\mathbf{y}\cdot\mathbf{z}),$$

$$U_4\equiv x^2(\mathbf{y}\cdot\mathbf{z})+y^2(\mathbf{x}\cdot\mathbf{z})+z^2(\mathbf{x}\cdot\mathbf{y})+2(\mathbf{x}\cdot\mathbf{y})(\mathbf{x}\cdot\mathbf{z})+2(\mathbf{x}\cdot\mathbf{y})$$
$$\times(\mathbf{y}\cdot\mathbf{z})+2(\mathbf{x}\cdot\mathbf{z})(\mathbf{y}\cdot\mathbf{z}). \tag{6.13}$$

For $\bar{I}=$n4 from Eq. (4.39), using the relations $P\mathbf{y}=0$, $P'\mathbf{x}=0$ in Eq. (6.9) one obtains

$$6\bar{A}_1=(\mathbf{x}P\mathbf{x})(\mathbf{y}P'\mathbf{z})+2(\mathbf{x}P\mathbf{z})(\mathbf{y}P'\mathbf{z})+(\mathbf{x}P\mathbf{z})(\mathbf{y}P'\mathbf{y}),$$

$$36\bar{A}_2=(d-1)\{U_1(\mathbf{y}P'\mathbf{z})+U_2(\mathbf{x}P\mathbf{z})+(\mathbf{x}P\mathbf{x})(\mathbf{y}\cdot\mathbf{z})$$
$$+(\mathbf{y}P'\mathbf{y})(\mathbf{x}\cdot\mathbf{z})+[\mathbf{z}(P+P')\mathbf{z}](\mathbf{x}\cdot\mathbf{y})\}+$$
$$+2\{U_1(\mathbf{y}P'P\mathbf{z})+U_2(\mathbf{x}PP'\mathbf{z})+U_3(\mathbf{x}PP'\mathbf{y})$$
$$+[\mathbf{z}(PP'+P'P)\mathbf{z}](\mathbf{x}\cdot\mathbf{y})\},$$

$$9\bar{A}_3=U_4\{(d-1)^2+2\,\mathrm{tr}(PP')\} \tag{6.14}$$

with U_1-U_4 from Eq. (6.13); $\mathrm{tr}(PP')$ is the trace of a matrix product.

Substituting the specific values for the vectors and projectors for any given diagram from Eqs. (6.8)–(6.11) into expressions (6.12)–(6.14) gives explicit expressions for the corresponding coefficients $\bar{A}_i$. Then, using the additional information from Eqs. (6.8)–(6.11) one obtains the desired expressions for the coefficients A_i for any diagram in the form of scalar integrals (4.41c). All these simple but cumbersome technical operations are easily performed by means of a computer.

Now let us turn to the factorizable diagrams Nos. 46, 51, 61. Diagram No. 46 factorizes to a product of two blocks Nos. 21, 22; diagram No. 51 factorizes to a product of the blocks Nos. 21, 31; diagram No. 61 factorizes to a product of three blocks No. 21. Since the quantities B_i for diagrams

Nos. 21, 22 already include their own symmetry coefficient 1/2, we conclude that, in order to obtain the needed symmetry coefficient in Fig. 1 for diagrams Nos. 46, 51, an additional symmetry coefficient [like C in Eq. (5.20)] is not needed, while for diagram No. 61 it should be taken to be 1/6.

Therefore, taking into account Eqs. (4.18) and (4.27), we obtain for diagrams Nos. 46, 51, 61,

diagram No. 46, $\Gamma=V_{1234}[B_1w_1w_2+B_2w^2\delta_{12}][B'_1w_3w_4$
$$+B'_2w^2\delta_{34}], \tag{6.15a}$$

diagram No. 51, $\Gamma=V_{12345}[B_1w_1w_2+B_2w^2\delta_{12}]$
$$\times[B'_1w_3w_4w_5+B'_2w^2\delta_{34}w_5], \tag{6.15b}$$

diagram No. 61, $\Gamma=[1/6]V_{123456}[B_1w_1w_2+B_2w^2\delta_{12}]$
$$\times[B_1w_3w_4+B_2w^2\delta_{34}][B_1w_5w_6$$
$$+B_2w^2\delta_{56}], \tag{6.15c}$$

where $B_{1,2}$ are the known coefficients for diagram No. 21, $B'_{1,2}$ in Eq. (6.15a) are the analogous coefficients for diagram No. 22, and $B'_{1,2}$ in Eq. (6.15b) are the coefficients for diagram No. 31.

Using the relations (4.36), from Eqs. (6.15) one obtains

$$\bar{\Gamma}\;(\text{diagram No. } 46)=k_1B_1B'_1+k_2(B_1B'_2+B_2B'_1)$$
$$+k_3B_2B'_2,$$

$$\bar{\Gamma}\;(\text{diagram No. } 51)=k_1B_1B'_1+k_2(B_1B'_2+B_2B'_1)$$
$$+k_3B_2B'_2,$$

$$\bar{\Gamma}\;(\text{diagram No. } 61)=[1/6][k_1B_1^3+3k_2B_1^2B_2+3k_3B_1B_2^2$$
$$+k_4B_2^3] \tag{6.16}$$

with the coefficients k_i known from Eq. (4.36c) for diagram No. 46, from Eq. (4.36d) for diagram No. 51, and from Eq.

(4.36e) for diagram No. 61. The relations (6.16) give the desired answers for the three-loop factorizable diagrams.

B. Calculation of the three-loop integrals and anomalous dimensions: General scheme

Substituting the specific values for the vectors and projectors, given in Eqs. (6.1), (6.3)–(6.6), (6.8)–(6.11) for all normal three-loop diagrams, into the general formulas (4.42), (4.43), (6.12)–(6.14) gives explicit expressions for the quantities $\bar{A}_i$ in Eq. (4.41c) for any diagram in the form of polynomials in the scalar products $(\mathbf{k} \cdot \mathbf{q})$, $(\mathbf{k} \cdot \mathbf{l})$, $(\mathbf{q} \cdot \mathbf{l})$ and moduli k, q, l of the vectors $\mathbf{k}, \mathbf{q}, \mathbf{l}$.

It is worth noting that for all the normal three-loop diagrams, the products $\phi_s \bar{A}_i$ have the form of sums of monomials in $\mathbf{k}, \mathbf{q}, \mathbf{l}$ of order six. In the variables "moduli angles," each of these monomials contains the factor l^2, which is canceled out by the analogous factor in the energy denominator $\epsilon_l = \nu l^2$ present in each of these diagrams. It is also worth noting that these products involve the modulus k in the power 2 or less (otherwise the integrals over k would be divergent).

In the three-loop diagrams, we only need the poles in ε, that is, the contributions of order ε^{-3}, ε^{-2}, and ε^{-1}. The following general scheme is used in their calculation.

(1) The integrands are expanded in the set of scalar products $(\mathbf{k} \cdot \mathbf{q})$, $(\mathbf{k} \cdot \mathbf{l})$, $(\mathbf{q} \cdot \mathbf{l})$; the results are represented as a multiple series in these quantities.

(2) Then, the angular averaging $\langle \cdots \rangle$ is performed with respect to the directions of the vectors $\mathbf{k}, \mathbf{q}, \mathbf{l}$, that is, the following quantities are calculated:

$$T_{n_1 n_2 n_3} = \langle (\mathbf{k} \cdot \mathbf{q})^{n_1} (\mathbf{k} \cdot \mathbf{l})^{n_2} (\mathbf{q} \cdot \mathbf{l})^{n_3} \rangle \tag{6.17}$$

with arbitrary integer exponents $n_i \geq 0$.

(3) The next step is the integration over the moduli k, q, l. All the needed integrals reduce to the form

$$\int_1^\infty \frac{dk}{k^{1+\varepsilon}} \int_1^\infty \frac{dq}{q^{1+\varepsilon}} \int_1^\infty \frac{dl}{l^{1+\varepsilon}} \frac{k^{2n_1} q^{2n_2} l^{2n_3}}{(k^2+q^2+l^2)^{n_4}(q^2+l^2)^{n_5}}, \tag{6.18}$$

where the integer exponents $n_i \geq 0$ satisfy the relation $n_1 + n_2 + n_3 = n_4 + n_5$, so that the integrals contain only logarithmic UV divergencies for $\varepsilon \to 0$. Only the pole parts are extracted from the integrals (6.18).

(4) The last step is the summation of the resulting series. They have the forms of a double infinite series with the coefficients given by n-fold finite sums ($n \leq 5$); the number of terms in the latter increases rapidly with the order of the coefficient. This summation is the only operation that cannot be performed exactly (analytically) and is therefore the only source of errors in numerical coefficients in expressions like Eqs. (1.13).

Of course, the straightforward but cumbersome operations listed above have been performed with the aid of a computer.

The first step, the expansion in the scalar products $(\mathbf{k} \cdot \mathbf{q})$, $(\mathbf{k} \cdot \mathbf{l})$, $(\mathbf{q} \cdot \mathbf{l})$, contains some conceptual subtleties and we shall discuss it in more detail. The problem is that the plain expansion of the integrands in the powers of the scalar products in some cases leads to a divergent series.

The nonpolynomial dependence of the integrands on the cosines of the angles appears only from the energy factors ϕ_E^{-1}, whose explicit forms are given in Eqs. (6.1), (6.3)–(6.6), (6.8)–(6.11). For all the diagrams, the nontrivial factors in ϕ_E have the forms $q^2 + l^2 + \text{const}\,(\mathbf{q} \cdot \mathbf{l})$ and $k^2 + q^2 + l^2 +$ some linear combination of all scalar products, and in the expansions in powers of the scalar products, the denominators will contain powers of the quantities $(q^2 + l^2)$ and $(k^2 + q^2 + l^2)$. Such expansions converge for all cofactors in ϕ_E^{-1}, which do not contain the "energy" $\epsilon_{\mathbf{k+q+l}}$ with the sum of all three momenta. The cofactors with $\epsilon_{\mathbf{k+q+l}}$ require special consideration. They are present in diagrams Nos. 23, 32, 33, 34, 42 and are proportional to the following factors:

$$\text{diagram No. 23,} \quad \phi_E^{-1} \propto \epsilon_{\mathbf{k+q+l}}^{-1} \propto [Q+2S]^{-1},$$

$$\text{diagram No. 32,} \quad \phi_E^{-1} \propto [\epsilon_{\mathbf{k}} + \epsilon_{\mathbf{q+l}} + \epsilon_{\mathbf{k+q+l}}]^{-1}$$

$$\propto [Q+S+(\mathbf{q} \cdot \mathbf{l})]^{-1},$$

$$\text{diagram No. 33,} \quad \phi_E^{-1} \propto [\epsilon_{\mathbf{q}} + \epsilon_{\mathbf{k+l}} + \epsilon_{\mathbf{k+q+l}}]^{-1}$$

$$\propto [Q+S+(\mathbf{k} \cdot \mathbf{l})]^{-1},$$

$$\text{diagram No. 34,} \quad \phi_E^{-1} \propto [\epsilon_{\mathbf{l}} + \epsilon_{\mathbf{k+q}} + \epsilon_{\mathbf{k+q+l}}]^{-1}$$

$$\propto [Q+S+(\mathbf{k} \cdot \mathbf{q})]^{-1},$$

$$\text{diagram No, 42,} \quad \phi_E^{-1} \propto [\epsilon_{\mathbf{k}} + \epsilon_{\mathbf{q}} + \epsilon_{\mathbf{l}} + \epsilon_{\mathbf{k+q+l}}]^{-1}$$

$$\propto [Q+S]^{-1}, \tag{6.19}$$

where $Q \equiv k^2 + q^2 + l^2$ and $S \equiv (\mathbf{k} \cdot \mathbf{q}) + (\mathbf{k} \cdot \mathbf{l}) + (\mathbf{q} \cdot \mathbf{l})$.

From the obvious identities $(\mathbf{k}+\mathbf{q}+\mathbf{l})^2 \geq 0$, $(\mathbf{k}-\mathbf{q})^2 + (\mathbf{k}-\mathbf{l})^2 + (\mathbf{q}-\mathbf{l})^2 \geq 0$, $|(\mathbf{k} \cdot \mathbf{q})| \leq kq$, $|(\mathbf{k} \cdot \mathbf{l})| \leq kl$, and $|(\mathbf{q} \cdot \mathbf{l})| \leq ql$, it follows that

$$-Q/2 \leq S \leq Q, \quad |(\mathbf{k} \cdot \mathbf{q})| \leq Q/2, \quad |(\mathbf{k} \cdot \mathbf{l})| \leq Q/2,$$

$$|(\mathbf{q} \cdot \mathbf{l})| \leq Q/2. \tag{6.20}$$

It then follows that the factor (6.19) in diagram No. 42 can be expanded in the powers of the ratio S/Q with $|S/Q| \leq 1$, while for No. 23 this is impossible: in the integration region, there is a subregion of the same dimension (namely, $3 \times d$) in which $2|S| > Q$. This difficulty can be circumvented by means of the shift of the point around which the expansion is made in diagram No. 23,

$$[Q+2S]^{-1} = [3Q/2 + (4S-Q)/2]^{-1}$$

$$= [2/3Q] \sum_{n=0}^\infty [(1-4S/Q)/3]^n. \tag{6.21}$$

The convergence of the series in Eq. (6.21) is ensured by the inequality $|(1-4S/Q)/3| \leq 1$, which follows from Eq. (6.20). The equality takes place only in the $(2 \times d)$-dimensional subregion $\mathbf{k}+\mathbf{q}+\mathbf{l} = 0$, which has zero measure in the $(3 \times d)$-dimensional integration region and

does not spoil the convergence of the corresponding series for the integral [similar considerations ensure the convergence of the series (5.35c) for the two-loop integral h].

For the factor (6.19) in diagram No. 32 the following shift can be used:

$$[Q+S+(\mathbf{q}\cdot\mathbf{l})]^{-1}=\{5Q/4+[S+(\mathbf{q}\cdot\mathbf{l})-Q/4]\}^{-1}$$

with the subsequent expansion in the powers of the ratio [$S+(\mathbf{q}\cdot\mathbf{l})-Q/4]/(5Q/4)$, whose modulus does not exceed unity owing to inequalities (6.20). Similar expansions (with obvious modifications) can be written for diagrams Nos. 33, 34.

Such infinite series contain additional finite sums originated from the powers of the expansion parameters, which have the forms ''constant + linear combination of the scalar products.'' It is clear that this summation should be performed in first, before all the other summations: only this order of summations ensures the convergence of the series.

Calculation of the angular integral (6.17) and momentum integral (6.18) is a separate task; it is discussed in the next two sections. The results for the coefficients A_i for all the normal three-loop diagrams are presented in the Appendix. The ε^{-3} contributions in all diagrams have been found analytically for general space dimensionality d (in order to calculate them, it is sufficient to neglect all the scalar products in the energy denominators ϕ_E), while the ε^{-2} and ε^{-1} parts have been found for the physical cases $d=2,3$ and in the large d limit; the results have been presented in Ref. [15] (of course, this calculation can be made for any fixed given value of d).

Now, using the standard scheme (see Sec. IV), one finds the three-loop contribution $[Z_F^{-1}]_3$ in the expansion (4.7) for the renormalization constant Z_F^{-1}. The anomalous dimension $\gamma_F \equiv \gamma_{nl}$ is given by the relation $\gamma_F = -\beta\partial_u\ln Z_F^{-1}$; see Eq. (3.4). Substituting Eqs. (2.17) and (4.7) into the last relation expresses the anomalous dimension in the coefficients $[Z_F^{-1}]_k$. Within our accuracy one obtains

$$\gamma_F(u)=[\varepsilon-u(d-1)/2d]\{[Z_F^{-1}]_1+2[Z_F^{-1}]_2-[Z_F^{-1}]_1^2$$
$$+3[Z_F^{-1}]_3-3[Z_F^{-1}]_1[Z_F^{-1}]_2+[Z_F^{-1}]_1^3\}. \quad (6.22)$$

Substituting the known expressions for $[Z_F^{-1}]_k$ into Eq. (6.22) gives the anomalous dimension $\gamma_F(u)$ to order u^3.

Since the quantity γ_F is UV finite, that is, finite at $\varepsilon=0$, the pole parts must cancel each other in Eq. (6.22). This implies some exact relations between the senior poles in the quantities $[Z_F^{-1}]_k$ with $k\geq2$ (ε^{-2} in $[Z_F^{-1}]_2$ and ε^{-2}, ε^{-3} in $[Z_F^{-1}]_3$) and the ε^{-1} parts of the previous orders in u. Such relations provide an additional possibility to control the absence of calculational errors. In fact, the knowledge of senior poles (ε^{-k} with $k\geq2$) is needed only to check this cancellation; the nonvanishing contributions in Eq. (6.22) are completely determined by the ε^{-1} terms in the quantities $[Z_F^{-1}]_k$. In the MS scheme, the anomalous dimension $\gamma_F(u)$ appears independent of ε; this is a consequence of the relation $Z_F=1+$ only poles in ε.

Finally, the relation (3.4) with u_* from Eq. (2.18) gives the $O(\varepsilon^3)$ results for the critical dimensions presented in Ref. [15] and Eqs. (1.13).

C. Angular integrations in the three-loop diagrams

The two-loop integrals (4.41b) involve only two vectors $\mathbf{k}$ and $\mathbf{q}$ and one angle ϑ between them, so that the procedure of the angular averaging reduces there to the only standard formula (5.24). The three-loop integrals (4.41c) involve three vectors $\mathbf{k}$, $\mathbf{q}$, and $\mathbf{l}$ and three angles between them, so that the calculation of the quantities (6.17) is not all that simple. Below we present the results of this calculation.

Obviously, the quantity (6.17) differs from zero only if all the three numbers $n_{1,2,3}$ are simultaneously even or odd. It is also clear that the quantity (6.17) is symmetrical with respect to any permutation of the exponents $n_{1,2,3}$, and with no loss of generality it can be assumed that n_2 is the minimal exponent,

$$n_2=\min\{n_1,n_2,n_3\} \quad (6.23)$$

[the notation in the formulas below is consistent with the assumption (6.23)].

The straightforward calculation (first, the averaging over the direction of one momentum, say $\mathbf{k}$, and then the averaging over the angle between the two remaining vectors $\mathbf{q}$ and $\mathbf{l}$) leads to the following result for the quantity (6.17):

$$T_{n_1n_2n_3}=k^{n_1+n_2}q^{n_1+n_3}l^{n_2+n_3}\bar{T}_{n_1n_2n_3}, \quad (6.24)$$

where the moduli of the vectors are isolated explicitly, and

$$\bar{T}_{n_1n_2n_3}=\alpha_{n_1+n_2}\alpha_{n_2+n_3}K(n_1,n_2)\widetilde{T}_{n_1n_2n_3} \quad (6.25)$$

with coefficients α_{2n} from Eq. (5.24) and

$$K(n_1,n_2)=\frac{2^{n_2}n_1![(n_1+n_2)/2]!}{(n_1+n_2)![(n_1-n_2)/2]!}$$

$$=\frac{(n_1-n_2+2)(n_1-n_2+4)\cdots(n_1+n_2)}{(n_1+1)(n_1+2)\cdots(n_1+n_2)},$$
$$(6.26)$$

$$\widetilde{T}_{n_1n_2n_3}=\sum_{k=0}^{n_2/2} Y_k,$$

$$Y_k=\frac{2^{-2k}n_2![(n_1-n_2)/2]!\alpha_{n_2+n_3-2k}}{k!(n_2-2k)![(n_1-n_2)/2+k]!\alpha_{n_2+n_3}}. \quad (6.27)$$

We recall that the numbers $n_{1,2,3}$ in these expressions have the same parity, and that n_2 is the minimal one according to Eq. (6.23). The upper limit in the sum (6.27) for odd n_2 is understood as the integer part of $n_2/2$.

The following special values and recurrent relations for the quantity K in Eq. (6.26) are useful:

$$K(m,0)=K(m,1)=1, \quad K(m,m)=m!/(2m-1)!!,$$

$$K(m+1,m+1)/K(m,m)=(m+1)/(2m+1),$$

$$K(m+2,n)/K(m,n)=(m+1)(m+2)/(m-n+2)$$

$$\times(m+n+1). \qquad (6.28)$$

For the terms Y_k in the sum (6.27) one has

$$Y_0=1,$$

$$Y_{k+1}/Y_k=\frac{(n_2-2k)(n_2-2k-1)(d+n_2+n_3-2k-2)}{2(k+1)(n_1-n_2+2k+2)(n_2+n_3-2k-1)}. \qquad (6.29)$$

Using these relations, the quantities (6.26) and (6.27) are easily calculated by a computer.

D. Modular integrations in the three-loop diagrams

Let us turn to the calculation of the three-loop integrals (6.18) over the moduli k,q,l, which arise as coefficients in the expansion of the quantities A_i in Eq. (4.41c) in the scalar products $(\mathbf{k}\cdot\mathbf{q}),(\mathbf{k}\cdot\mathbf{l}),(\mathbf{q}\cdot\mathbf{l})$; see Sec. VI B. For the complete three-loop calculation, it is sufficient to know some special cases of the general integral (6.18), which we denote I_1-I_9 in what follows. Below we give the explicit answers for these intergals, with the precise specification of the indices n_1-n_5, and then turn to the derivation. Only the pole parts ε^{-3}, ε^{-2}, and ε^{-1} of these integrals are given, which is sufficient for the calculation of the quantities A_i within our accuracy. We shall use the notation

$$I\{F\}\equiv\int_1^\infty\frac{dk}{k^{1+\varepsilon}}\int_1^\infty\frac{dq}{q^{1+\varepsilon}}\int_1^\infty\frac{dl}{l^{1+\varepsilon}}F \qquad (6.30)$$

for any function $F=F(k,q,l)$. The integrals I_1-I_9 are as follows:

$$I_1\equiv I\left\{\frac{k^{2n_1}q^{2n_2}l^{2n_3}}{(k^2+q^2+l^2)^{n_4}(q^2+l^2)^{n_5}}\right\}$$

$$=\frac{(n_1-1)!(n_2-1)!(n_3-1)!(n_4-n_1-1)!}{12\varepsilon\,(n_4-1)!(n_2+n_3-1)!} \qquad (6.31)$$

with $n_1+n_2+n_3=n_4+n_5$, $n_4>n_1$, $n_{1,2,3,4}>0$, and $n_5\geq0$;

$$I_2\equiv I\left\{\frac{q^{2n_2}l^{2n_3}}{(k^2+q^2+l^2)^{n_4}(q^2+l^2)^{n_5}}\right\}$$

$$=\frac{(n_2-1)!(n_3-1)!}{12(n_2+n_3-1)!}\left[\frac{1}{\varepsilon^2}+\frac{1}{\varepsilon}\left(\sum_{k=1}^{n_2+n_3-1}\frac{1}{k}-\sum_{k=1}^{n_4-1}\frac{1}{k}-\frac{1}{2}\right.\right.$$

$$\left.\left.\times\sum_{k=1}^{n_2-1}\frac{1}{k}-\frac{1}{2}\sum_{k=1}^{n_3-1}\frac{1}{k}\right)\right] \qquad (6.32)$$

with $n_2+n_3=n_4+n_5$, $n_{2,3,4}>0$, and $n_5\geq0$ [in Eq. (6.32) and all the formulas below, any sum with the upper limit lesser than the lower one is understood as equal to zero];

$$I_3\equiv I\left\{\frac{k^{2n_1}q^{2n_2}}{(k^2+q^2+l^2)^{n_4}}\right\}$$

$$=\frac{(n_1-1)!(n_2-1)!}{12(n_4-1)!}\left[\frac{1}{\varepsilon^2}-\frac{1}{2\varepsilon}\left(\sum_{k=1}^{n_1-1}\frac{1}{k}+\sum_{k=1}^{n_2-1}\frac{1}{k}\right)\right] \qquad (6.33)$$

with $n_1+n_2=n_4$ and $n_{1,2}>0$;

$$I_4\equiv I\left\{\frac{k^{2n_1}q^{2n_2}}{(k^2+q^2+l^2)^{n_4}(q^2+l^2)}\right\}$$

$$=\frac{(n_1-1)!(n_2-2)!}{12\varepsilon(n_4-1)!}\left[\frac{1}{\varepsilon^2}-\frac{1}{2\varepsilon}\right.$$

$$\left.\times\left\{\frac{2}{(n_2-1)}+\sum_{k=1}^{n_1-1}\frac{1}{k}+\sum_{k=1}^{n_2-2}\frac{1}{k}\right\}\right] \qquad (6.34)$$

with $n_1+n_2=n_4+1$, $n_1>0$, and $n_2>1$;

$$I_5\equiv I\left\{\frac{k^2}{(k^2+q^2+l^2)}\left(\frac{ql}{q^2+l^2}\right)^{2n}\right\}$$

$$=\frac{[(n-1)!]^2}{12(2n-1)!}\left[\frac{2}{\varepsilon^2}-\frac{1}{\varepsilon}\left(3\mathcal{B}_{n-1}+\sum_{k=n}^{2n-1}\frac{1}{k}\right)\right] \qquad (6.35)$$

with $n>0$ and $\mathcal{B}_n$ from Eq. (5.34);

$$I_6\equiv I\left\{\frac{k^2q^{2(n+1)}l^{2n}}{(k^2+q^2+l^2)(q^2+l^2)^{2n+1}}\right\}=\frac{1}{2}I_5; \qquad (6.36)$$

$$I_7\equiv I\left\{\frac{k^2}{k^2+q^2+l^2}\right\}=\frac{1}{3\varepsilon^3}; \qquad (6.37)$$

$$I_8\equiv I\left\{\frac{k^2q^2}{(k^2+q^2+l^2)(q^2+l^2)}\right\}=\frac{1}{6\varepsilon^3}; \qquad (6.38)$$

$$I_9\equiv I\left\{\frac{q^4}{(k^2+q^2+l^2)(q^2+l^2)}\right\}=\frac{1}{3\varepsilon^3}-\frac{1}{12\varepsilon^2}-\frac{1}{12\varepsilon}. \qquad (6.39)$$

Now let us turn to the derivation of expressions (6.31)–(6.39). The integrals $I_{1,2}$ can be obtained from the generation function

$$R(a,b;m)\equiv\int_m^\infty\frac{dk}{k^{1+\varepsilon}}\int_m^\infty\frac{d\rho}{\rho^{1+2\varepsilon}}\frac{\rho^2}{(ak^2+b\rho^2)}$$

$$=\frac{m^{-3\varepsilon}}{6b}\left[\frac{1}{\varepsilon^2}+\frac{1}{\varepsilon}\ln(b/a)+O(1)\right]. \qquad (6.40)$$

We shall also need the first terms of the ε expansion of the integral

$$J(p,q) \equiv \int_0^{\pi/2} d\varphi (\cos\varphi)^{2p-1-\varepsilon} (\sin\varphi)^{2q-1-\varepsilon}$$

$$= \frac{\Gamma(p-\varepsilon/2)\Gamma(q-\varepsilon/2)}{2\Gamma(p+q-\varepsilon)}$$

$$= \frac{\Gamma(p)\Gamma(q)}{2\Gamma(p+q)} \left\{ 1 + \varepsilon \left[\psi(p+q) - \frac{1}{2}\psi(p) - \frac{1}{2}\psi(q) \right] \right\}$$

$$+ O(\varepsilon^2)$$

$$= \frac{(p-1)!(q-1)!}{2(p+q-1)!} \left[1 + \varepsilon \left(\sum_{k=1}^{p+q-1} \frac{1}{k} - \frac{1}{2} \sum_{k=1}^{p-1} \frac{1}{k} \right. \right.$$

$$\left. \left. - \frac{1}{2} \sum_{k=1}^{q-1} \frac{1}{k} \right) \right] + O(\varepsilon^2), \tag{6.41}$$

where $\Gamma(z)$ is the Euler gamma function and $\psi(z) = d \ln \Gamma(z)/dz$.

The calculation of the quantity $R \equiv R(a,b;m) = m^{-3\varepsilon} R(a,b;1)$ is similar to the derivation of Eq. (5.33). The operation $\mathcal{D}_m \equiv m \partial/\partial m$ is applied to the double integral in Eq. (6.40), which reduces it to the sum of two single integrals and explicitly isolates the pole factor ε^{-1},

$$R = -\frac{1}{3\varepsilon} \mathcal{D}_m R$$

$$= \frac{m^{-3\varepsilon}}{3\varepsilon} \left[\int_1^\infty dk \frac{1}{k^{1+\varepsilon}(ak^2+b)} + \int_1^\infty \frac{d\rho}{\rho^{1+2\varepsilon}} \frac{\rho^2}{(a+b\rho^2)} \right].$$

Now one can set $\varepsilon=0$ in the integral over k (it remains finite at $\varepsilon=0$). The pole in ε in the integral over ρ comes from large ρ and it can be isolated explicitly,

$$\int_1^\infty \frac{d\rho}{\rho^{1+2\varepsilon}} \frac{\rho^2}{(a+b\rho^2)} = \frac{1}{b} \int_1^\infty \frac{d\rho}{\rho^{1+2\varepsilon}} - \frac{a}{b} \int_1^\infty \frac{d\rho}{\rho^{1+2\varepsilon}} \frac{1}{(a+b\rho^2)}$$

$$= \frac{1}{2b\varepsilon} - \frac{a}{b} \int_1^\infty \frac{d\rho}{\rho(a+b\rho^2)} + O(\varepsilon),$$

which immediately leads to the answer (6.40).

In the integral I_1 the pole contribution comes from the part of the integration region where all three momenta k,q,l simultaneously tend to infinity, and in I_2 there is also a pole contribution coming from the subregion where q,l simultaneously tend to infinity at fixed finite k. This means that the pole parts of the integrals $I_{1,2}$ are not affected if one changes to the polar coordinates ρ, φ ($q = \rho\cos\varphi$, $l = \rho\sin\varphi$) with the integration region $0 \le \varphi \le \pi/2$, $1 \le \rho < \infty$, that is, the following replacement is performed:

$$\int_1^\infty dq \int_1^\infty dl \cdots \rightarrow \int_0^{\pi/2} d\varphi \int_1^\infty \rho d\rho \cdots.$$

The integration regions in these two expressions are not identical, but the values of integrals differ only by an unessential contribution, finite at $\varepsilon \to 0$. For I_1 this gives

$$I_1 = \int_0^{\pi/2} d\varphi (\cos\varphi)^{2n_2-1-\varepsilon} (\sin\varphi)^{2n_3-1-\varepsilon}$$

$$\times \int_1^\infty \frac{dk}{k^{1+\varepsilon}} \int_1^\infty \frac{d\rho}{\rho^{1+2\varepsilon}} \frac{k^{2n_1}\rho^{2n_4-2n_1}}{(k^2+\rho^2)^{n_4}}.$$

This integral can be expressed using $J(p,q)$ from Eq. (6.41) and the derivative of the generating function $R(a,b;m)$ from Eq. (6.40) as follows:

$$I_1 = [(n_4-1)!]^{-1} J(n_2,n_3)(-\partial_a)^{n_1}$$

$$(-\partial_b)^{n_4-n_1-1} R(a,b;1)|_{a=b=1} \tag{6.42}$$

with $\partial_a = \partial/\partial a$, $\partial_b = \partial/\partial b$, which immediately leads to the answer (6.31). Note that the ε^{-2} contribution in R depends only on b [see Eq. (6.40)] and therefore vanishes in the above expression owing to the differentiation with respect to a (we recall that $n_1 > 0$ for I_1). Although the integral I_2 is formally given by expression (6.42) with $n_1 = 0$,

$$I_2 = [(n_4-1)!]^{-1} J(n_2,n_3)(-\partial_b)^{n_4-1} R(1,b;1)|_{b=1}, \tag{6.43}$$

the ε^{-2} part of the function (6.40) survives in Eq. (6.43) owing to the absense of the derivative ∂_a, so that the $O(\varepsilon)$ contributions should be taken into account in the integral (6.41). This explains the sharp difference between the final expressions (6.31) and (6.32) for the integrals I_1 and I_2.

The relations (6.33)–(6.36) follow easily from Eqs. (6.31) and (6.32). The result (6.33) for I_3 is obtained from Eq. (6.32) at $n_5 = 0$ using the symmetries of the integrand. In its turn, the result (6.34) for I_4 follows from Eqs. (6.31) and (6.33) if the obvious identity $q^{2n_2}/(q^2+l^2) = q^{2(n_2-1)} - q^{2(n_2-1)}l^2/(q^2+l^2)$ is substituted on its left-hand side. The result (6.35) for I_5 is obtained using the substitution $k^2/(k^2+q^2+l^2) = 1 - (q^2+l^2)/(k^2+q^2+l^2)$: in the first term, the integral over k is trivial and the remaining integrations over q,l are performed using Eqs. (5.30), (5.33), and (5.34), while the second term reduces to I_2. The integral I_6 in Eq. (6.36) reduces to I_5 after the symmetrization of the integrand with respect to q,l.

The results (6.37) and (6.38) follow from the obvious relation $I\{1\} = \varepsilon^{-3}$ in Eq. (6.30) after the symmetrization of the integrands with respect to k,q,l. The last relation (6.39) is obtained using the substitution $q^2/(q^2+l^2) = 1 - l^2/(q^2+l^2)$: the first term coincides with I_7 and the second one is given by I_2 with $n_2 = n_3 = n_4 = n_5 = 1$.

E. Anomalous exponents at large d

In this section, we shall briefly discuss the behavior of the coefficients $\Delta_{nl}^{(k)}$ in the expansion (1.10) for $d \to \infty$. The model (1.1)–(1.3) has no finite upper critical dimension, above which the anomalous scaling vanishes. It disappears for infinite d [28], but reveals itself in the $O(1/d)$ approximation [6]. This fact confirms the relevance of the large d expansions for the issue of anomalous scaling; see also Refs. [29,30] for the discussion of the Navier-Stokes problem.
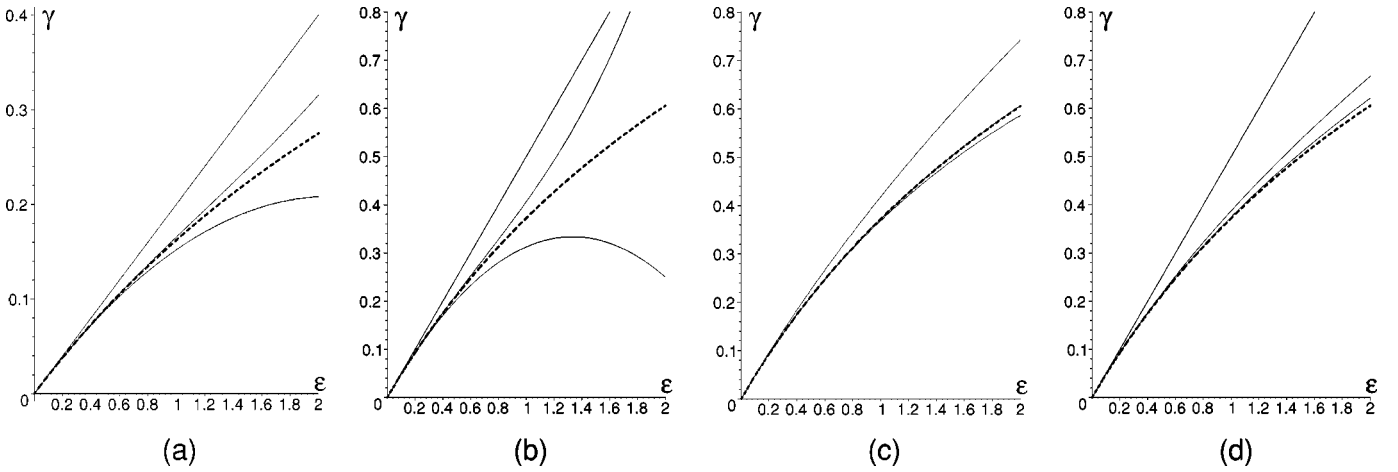
FIG. 3. Anomalous dimension $\gamma \equiv \gamma_{22}^*$ for $d=3$ (a) and $d=2$ (b)–(d). Dashed line: exact solution by Refs. [6,31]. Solid lines in (a) and (b): first, third, and second approximations of the plain ε expansion (from above to below). Solid lines in (c): first, third, and second approximations of the improved x expansion (from above to below; the third approximation is practically indistinguishable from the exact solution for all $0<\varepsilon<2$). Solid lines in (d): first, second, and third approximations of the inverse γ expansion (from above to below).

It follows from Eqs. (5.24) that for $d \to \infty$, the angular averages $\alpha_{2n} \equiv \langle \cos^{2n} \vartheta \rangle$ behave as $\alpha_{2n} \propto d^{-n}$ (each additional factor $\cos^2 \vartheta$ introduces additional smallness in $1/d$). Then from Eqs. (6.24)–(6.27) for the averages (6.17), one obtains $T_{n_1 n_2 n_3} \propto d^{-(n_1+n_2+n_3)/2}$ for $n_{1,2,3}$ even and $T_{n_1 n_2 n_3} \propto d^{-(n_1+n_2+n_3+1)/2}$ for $n_{1,2,3}$ odd. This means that, in order to find the behavior of the coefficients A_i for large d to any given finite order in $1/d$, one needs to take into account only *finite* number of terms in the expansion of the integrands in Eq. (4.37b) in the scalar product $(\mathbf{k} \cdot \mathbf{q})$, and integrands in Eq. (4.37c) in the set of scalar products $(\mathbf{k} \cdot \mathbf{q})$, $(\mathbf{k} \cdot \mathbf{l})$, $(\mathbf{q} \cdot \mathbf{l})$.

The d dependence of the coefficient $\Delta_{nl}^{(1)}$ in Eq. (1.10) is known from Eq. (1.11), while the quantities $\Delta_{nl}^{(2)}$, $\Delta_{nl}^{(3)}$ can be found as a series in $1/d$ to any given order as explained above. For general n and l to order $1/d^2$, we have obtained

$$\Delta_{nl} = \varepsilon[-n(n-2)(1-2/d)/2d + (l/2)(1-2/d+l/d+2/d^2)]$$
$$+ 3\varepsilon^2(n-2)(n-l)/4d^2 + \varepsilon^3(n-l)[1.749\,88(n-2)$$
$$- 0.624\,916l]/d^2 + O(\varepsilon^4). \tag{6.44}$$

Note that the ε^2 and ε^3 contributions decay for $d \to \infty$ faster than $1/d$ in agreement with the $O(1/d)$ result obtained in Ref. [6] for Δ_{n0}. Moreover, from Eq. (6.44) it follows that the leading $O(1/d^2)$ terms in these contributions vanish for $n=l$, so that the decay at $d \to \infty$ becomes even faster. For $n=l$ we have obtained

$$\Delta_{nn} = \varepsilon n/2 + n(n-1)\{\varepsilon/(d-1)(d+2) - \varepsilon^2[1+(2n$$
$$-7)/d]/d^3 - \varepsilon^3(3n-8)/2d^4\} + O(\varepsilon^4) \tag{6.45}$$

with the accuracy of $O(1/d^4)$.

VII. CONVERGENCE OF THE ε EXPANSION, INVERSE ε EXPANSION, AND COMPARISON WITH NONPERTURBATIVE RESULTS

An important issue that can be discussed on the example of the rapid-change model is that of the nature and conver-

gence of ε expansions in models of turbulence and the possibility of their extrapolation to finite values of $\varepsilon \sim 1$. The knowledge of the three terms of the ε expansion in model (1.1)–(1.3) allows one to discuss its convergence properties and to obtain improved predictions for finite ε, in reasonable agreement with the existing nonperturbative results: analytical solution of the zero-mode equations for $n=2$ [6], numerical solutions for $n=3$ [7], and numerical experiments for $n=4$ [23,24] and $n=6$ [25].

In Figs. 3(a) and 3(b), we show the anomalous dimension $\gamma \equiv \gamma_{22}^* \equiv \gamma_{22}(u_*)$ for $d=3$ (a) and 2 (b) in the $O(\varepsilon)$, $O(\varepsilon^3)$, and $O(\varepsilon^2)$ approximations (from above to below); the latter two obtained as simple sums of two and three terms of the ε expansion, respectively. The dashed line corresponds to the exact solution by Ref. [6]; see also Ref. [31] for the special cases $d=2$ and 3. Analogous diagrams for the cases $n=3$, $l=1$ and $n=4$, $l=0$ can be found in Ref. [15].

All these figures show that the agreement between the ε expansion and nonperturbative results for small ε improves when the higher-order terms are taken into account, but the deviation becomes remarkable for $\varepsilon \sim 1$ and decreasing d. Furthermore, the convergence of the ε series appears more irregular for $d=2$, while the forms of the nonperturbative results are not much affected by the choice of d.

Such behavior can be naturally understood by the example of the exact analytical result for $\gamma \equiv \gamma_{22}^*$ [6], which can be written in the form

$$2\gamma = -(d+2+\varepsilon) + \sqrt{(\varepsilon+\varepsilon_+)(\varepsilon+\varepsilon_-)},$$

$$\varepsilon_\pm = [d^2+d+2 \pm \sqrt{8d(d+1)}]/(d-1) \tag{7.1}$$

with $\varepsilon_+ \varepsilon_- = (d+2)^2$. It is useful to rewrite the smaller quantity ε_- in the form

$$\varepsilon_- = (d-1)\{1+[1+3d+\sqrt{8d(d+1)}]^{-1}\}. \tag{7.2}$$

From these expressions it follows that the corresponding ε expansion has the finite radius of convergence ε_-, ranging

from 0 to ∞ when d varies from 1 to ∞ (in particular, $\varepsilon_- \simeq 1.1$, $\varepsilon_+ \simeq 14.5$ for $d=2$, and $\varepsilon_- \simeq 2.1$, $\varepsilon_+ \simeq 11.9$ for $d=3$). Hence, the naive summation of the ε expansion for γ works only in the interval $\varepsilon < \varepsilon_-$, which decreases almost linearly with $(d-1)$. Since the singularity in Eq. (7.1) occurs for negative ε, it affects strongly the convergence of the ε expansion but is not ''visible'' in the form of the exact curve for positive ε, in contrast with the singularities occurring at $\varepsilon = 2$ in higher-order critical dimensions [7,8,23,24].

Therefore, in order to recover the behavior of γ from its ε series for larger ε, it is necessary to isolate explicitly the singularity at $\varepsilon = -\varepsilon_-$ in Eq. (7.1), thus changing it to a kind of improved ε expansion, whose radius of convergence is determined by a more distant singularity. This can be done, for example, by introducing the new expansion parameter $x = \sqrt{\varepsilon + \varepsilon_-} - \sqrt{\varepsilon_-}$, that is, $\varepsilon = x^2 + 2x\sqrt{\varepsilon_-}$. Then Eq. (7.1) can be written in the form

$$2\gamma = -(d+2+2x\sqrt{\varepsilon_-}+x^2)+(x+\sqrt{\varepsilon_-})$$
$$\times \sqrt{x^2+2x\sqrt{\varepsilon_-}+\varepsilon_+}. \qquad (7.3)$$

The convergence radius of the expansion in x is found from the equation $x^2 + 2x\sqrt{\varepsilon_-} + \varepsilon_+ = 0$ with the solutions $x_\pm = -\sqrt{\varepsilon_-} \pm i\sqrt{\varepsilon_+ - \varepsilon_-}$ and is therefore equal to $|x_\pm| = \sqrt{\varepsilon_+}$. For positive x and ε, this corresponds to the convergence for $0 < x < \sqrt{\varepsilon_+}$ or, equivalently, $0 < \varepsilon < \varepsilon_+ + 2\sqrt{\varepsilon_- \varepsilon_+} = \varepsilon_+ + 2(d+2)$.

The improvement of the convergence is illustrated by Fig. 3(c), where the exact exponent γ for $d=2$ is shown as a function of ε along with its first (x), second (x and x^2), and third (x, x^2 and x^3) orders of the improved x expansion, in which the variable x is also expressed as a function of ε. One can see that the convergence of the x expansion appears more regular and that its third-order approximation is hardly distinguishable from the exact result for all $0 < \varepsilon < 2$ (for $d=3$, the agreement is even better and for this reason is not shown). It should be stressed that it was not the existence of the exact solution or explicit form of the substitution $x(\varepsilon)$ that was crucial for the improvement but the knowledge of
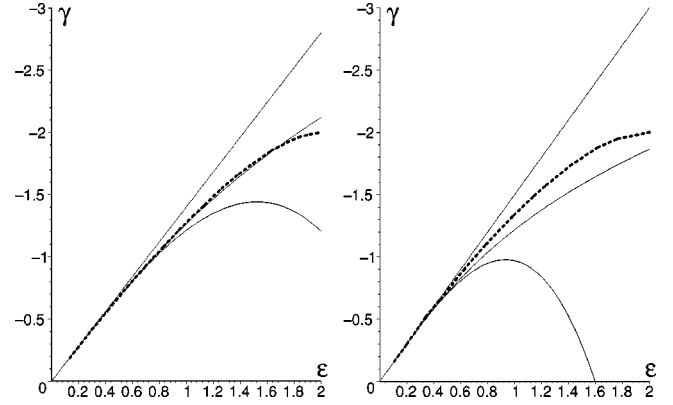

FIG. 4. Anomalous dimension $\gamma \equiv \gamma^*_{31}$ for $d=3$ (left) and $d=2$ (right): the $O(\varepsilon)$ approximation, the third-order approximation of the inverse γ expansion, and the third-order approximation of the plain ε expansion (from above to below). Dashed line: numerical solution by Refs. [7].

the character and location of the singularity, which determines the convergence properties of the plain ε expansion.

The difference with the models of critical phenomena, where ε series are always asymptotical, can be traced back to the fact that in the rapid-change models, there is no factorial growth of the number of diagrams in higher orders of the perturbation theory. The divergence for $d \to 1$ is naturally explained by the fact that the transverse vector field does not exist in one dimension. We also recall that the RG fixed point diverges at $d=1$, see Eq. (2.18), so that the coefficients of the ε series diverge for all dimensions Δ_{nl}.

It is then natural to assume that the ε series for all Δ_{nl} also have finite radii of convergence with the behavior similar to that of ε_- in Eq. (7.2). Therefore, in order to improve their convergence and to obtain reasonable predictions for finite values of ε, one should augment plain ε expansions by the information about the character of the singularities and their location in the complex ε plane. Such information can be extracted from the asymptotical behavior of the coefficients $\Delta_{nl}^{(k)}$ in Eq. (1.10) at large k. To our knowledge, the large k behavior of the ε series remains an open problem for
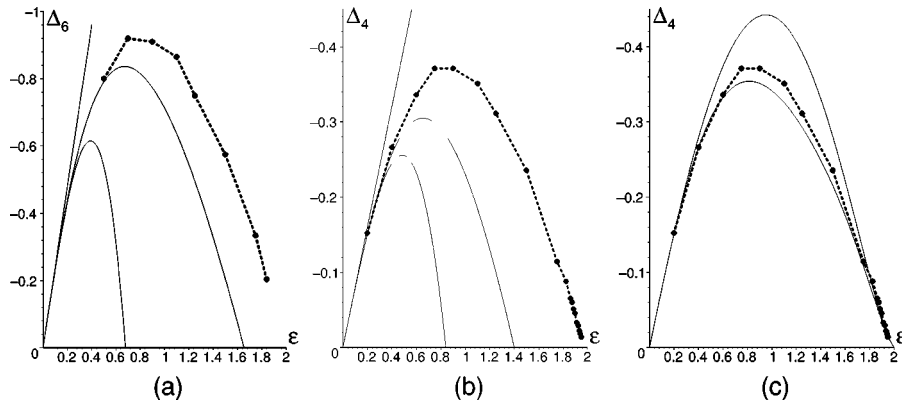

FIG. 5. Critical dimensions Δ_n for $d=3$: $n=6$ (a) and $n=4$ (b,c). Dots connected by dashed lines: numerical simulations by Refs. [25] ($n=6$) and [23,24] ($n=4$). Solid lines in (a,b): the $O(\varepsilon)$ slope, third-order approximation of the γ expansion, and third-order approximation of the plain ε expansion (from above to below). Solid lines in (c): approximations for $n=4$, obtained using the interpolation formula (7.5) with $p=1$ (upper curve) and $p=3$ (lower curve).

TABLE I. Coefficients $A_i^{(1,2)}$ for $d=2$.

Diagram No.	$A_1^{(2)}$ (units of 10^{-3})	$A_1^{(1)}$ (units of 10^{-3})	$A_2^{(2)}$ (units of 10^{-3})	$A_2^{(1)}$ (units of 10^{-3})	$A_3^{(2)}$ (units of 10^{-3})	$A_3^{(1)}$ (units of 10^{-3})
23	0.23875	−0.06103	0	0		
32	−0.56396	0.32532	0.49056	−0.56645		
33	1.11953	−0.49834	0.93382	−1.04911		
34	−1.05470	−0.12495	0.2434	−0.5770		
35	−0.41468	0.30671	−0.63626	0.22330		
42	−0.00053	−0.11026	0.06564	−0.16222	−0.54061	0.32914
43	0.02902	0.00249	0.03161	−0.00715	−0.33590	0.07208
44	−0.03113	−0.01477	0.03350	−0.00286	−0.19626	0.21410
45	−0.26802	0.26530	−0.02352	0.03554	0.88599	−0.88934

any dynamical model; the instanton analysis developed in Refs. [32] has mostly been concentrated on the behavior of the exponents in the limit $n \to \infty$. One can hope that the implementation of the instanton calculus within the RG framework will give the solution of this important problem.

It turns out, however, that certain elementary considerations allow one to improve the convergence of the ε series and, at the same time, to achieve a better agreement with the nonperturbative results. Let us explain the idea of the improvement by the example of the exact solution (7.1). We express ε as a function of the exponent γ using Eq. (7.1) and expand the right-hand side of the resulting exact relation

$$\varepsilon = \gamma(d-1)(d+2+\gamma)/[2-\gamma(d-1)] \qquad (7.4)$$

in γ; this gives the "inverse γ expansion." It is easy to see that, for $\varepsilon \sim 1$ and physical dimensions $d=2$ and 3, the respective values of γ lie within the region of convergence of the inverted series: $\gamma < 2/(d-1)$. The improvement of the convergence is also seen from Fig. 3(d), where the exponent $\gamma = \gamma_{22}^*$ for $d=2$ is shown as a function of ε along with the first (γ), second (γ and γ^2), and third (γ, γ^2, and γ^3) orders of the γ expansion, expressed in the original variable ε: the approximate curves approach the exact curve from the same side and represent the exact result (7.1) much better than the corresponding approximations of the plain ε expansion. The improvement is even better for $d=3$.

A simple explanation of the improvement follows. The convergence radius for the direct ε series is determined by the singularity on the right-hand side of Eq. (7.1), closest to

the origin, that is, $\varepsilon_c = -\varepsilon_-$. This *square-root* singularity disappears in the inverse relation (7.4), that is, the dependence of ε on γ in the vicinity of the corresponding point $2\gamma_c = -d-2-\varepsilon_c = -d-2+\varepsilon_-$ becomes analytic. This would also happen for any singularity of the form $\gamma - \gamma_c \propto (\varepsilon - \varepsilon_c)^{1/k}$ with any integer $k \geq 0$.

We assume that these features are also typical to the higher-order dimensions Δ_{nl} and construct the corresponding γ expansions. It is important here that $\gamma \equiv \gamma_{nl} = O(\varepsilon)$, so that there is a one-to-one correspondence between these two expansions and three terms of the γ expansion can be immediately obtained from Eqs. (1.7), (1.12), and (1.13). This simple procedure leads to a remarkable improvement of the convergence and, at the same time, the agreement with the numerical results, as is easily seen from Figs. 4 and 5.

In Fig. 4, we show the anomalous dimension $\gamma \equiv \gamma_{31}^*$ for $d=3$ (left) and $d=2$ (right): the $O(\varepsilon)$ approximation, the third-order approximation of the inverse γ expansion, and the third-order approximation of the plain ε expansion (from above to below); the dashed lines represent the exact numerical solution by Refs. [7] ($\gamma = \lambda - 3$ in the notation of [7]).

In Figs. 5(a) and 5(b), we show the quantities $\Delta_n \equiv \Delta_{n0}$ in three dimensions for $n=6$ (a) and $n=4$ (b): the $O(\varepsilon)$ slope, the third-order approximation of the γ expansion, and the third-order approximation of the plain ε expansion (from above to below); the dots connected by dashed lines represent the results of the numerical simulations by Refs. [25] ($n=6$) and [23,24] ($n=4$).

In all these cases, the improvement in the agreement with nonperturbative results is obvious. It should be emphasized,

TABLE II. Coefficients $A_i^{(1,2)}$ for $d=3$.

Diagram No.	$A_1^{(2)}$ (units of 10^{-3})	$A_1^{(1)}$ (units of 10^{-3})	$A_2^{(2)}$ (units of 10^{-3})	$A_2^{(1)}$ (units of 10^{-3})	$A_3^{(2)}$ (units of 10^{-3})	$A_3^{(1)}$ (units of 10^{-3})
23	1.03775	−0.14683	0	0		
32	−0.52289	0.39815	0.21884	−0.50345		
33	1.57028	0.00156	1.56822	−0.76955		
34	−1.64375	−0.82315	−0.43185	−1.46450		
35	−0.43289	0.51544	−1.07015	0.37916		
42	−0.07198	−0.08409	0.02952	−0.22968	−0.83453	0.37471
43	0.02808	0.00152	0.03587	−0.01186	−0.62532	0.07298
44	−0.07726	0.01392	0.00504	0.02341	−0.36121	0.37991
45	−0.33881	0.33509	−0.10389	0.11756	0.94431	−0.95923

TABLE III. Coefficients $a_i(d)$ for general d.

Diagram No.	$a_1(d)$	$a_2(d)$	$a_3(d)$
23	$9(d+1)(2d^2+2d-5)$	$27(d-1)^2(d+2)^2$	
32	$6(d+1)(d^2+d-3)$	$2(d^4+3d^3-3d^2-7d+10)$	
33	$-12(d+1)$	$-4(d^2+2d-2)$	
34	$3(d+1)(3d^2+3d-8)$	$3d^4+8d^3-13d^2-22d+32$	
35	$-12(d+1)$	$-4(d^2+2d-2)$	
42	$3(d+1)(d^2+d-8)/4$	$(d^4+6d^3+5d^2-16d+32)/8$	$-4(d^2+2d-2)$
43	$-6(d+1)$	$(d^3+d^2-4d+8)/2$	$d^4+4d^3+d^2-6d+8$
44	$-6(d+1)$	$(d^3+d^2-4d+8)/2$	$d^4+4d^3+d^2-6d+8$
45	$3(d+1)(d^2+d-8)/4$	$(d^4+6d^3+5d^2-16d+32)/8$	$-4(d^2+2d-2)$

however, that even the plain ε expansion captures some qualitative features of the dimensions Δ_n established in the numerical simulations [23–25]: the quantity $|\Delta_n|$ increases with ε, achieves a maximum at some point inside the interval $0 < \varepsilon < 2$, and then decreases to zero; the height of the maximum increases and its position moves to the left as n grows from 4 to 6 or d decreases from 3 to 2 ($\zeta_{2n} - n\zeta_2 = \Delta_{2n}$ in the notation of Refs. [23–25]).

It is no surprise, of course, that the disagreement between the perturbative and nonperturbative results becomes rather strong for $\varepsilon > 1$; this can be explained, for example, by the effect of the singularity at $\varepsilon = 2$ in the exact solutions [7,8,23,24] and by insufficient number of the known terms in the ε and γ series. For the case $n = 4$, $d = 3$, the situation can be improved by an interpolation formula that takes into account the first terms of the ε expansion along with the asymptotical behavior of the dimension Δ_4 in the vicinity of the opposite edge $\varepsilon = 2$, known from the numerical simulation [23,24]: $\Delta_4 = -[0.06(2-\varepsilon) + 1.13(2-\varepsilon)^{3/2}]$. In particular, one can choose

$$\Delta_4 = -[c_1\varepsilon + c_2\varepsilon^2 + c_3\varepsilon^3 + \cdots + c_k\varepsilon^k + \cdots][0.06(2-\varepsilon) + 1.13(2-\varepsilon)^{3/2}]. \tag{7.5}$$

The first coefficients $c_1 - c_p$ are determined by the requirement that the expansion in ε of the right-hand side of Eq. (7.5) reproduces the first p terms of the ε expansion for Δ_4, known from the RG (therefore, in practice one can only take $p \leq 3$). The values of these coefficients, once determined, will not change if one takes a larger value of p. The remaining coefficients c_k with $k > p$ should be chosen to reproduce the correct behavior at $\varepsilon \to 2$. The simplest possibility is to set $c_k = 0$ for all $k > p + 1$; then the last remaining coefficient c_{p+1} is unambiguously determined by the relation ($2c_1 + 4c_2 + 8c_3 + \cdots + 2^{p+1}c_{p+1}) = 1$ [the $O(2-\varepsilon)$ terms in the expression in the first square brackets produce only corrections of order $(2-\varepsilon)^2$ to the behavior of the right-hand of Eq. (7.5) side at $\varepsilon \to 2$ and thus should be neglected]. This procedure gives $c_1 = 0.241$, $c_2 = 0.129$ for $p = 1$ [upper curve in Fig. 5(c)] and $c_1 = 0.241$, $c_2 = 0.168$, $c_3 = -0.225$, $c_4 = 0.103$ for $p = 3$ (lower curve). One can see that the inclusion of the higher orders of the ε expansion improves remarkably the agreement with the ''experimental'' results of Refs. [23,24], shown in Fig. 5(c) by the dots connected by

dashed lines. It is also worth noting that the value of the coefficient c_2 for $p = 1$ (determined by the behavior at $\varepsilon \to 2$) appears rather close to its value for $p = 3$ (determined by the ε expansion), which demonstrates the robustness of the results obtained by the above procedure.

VIII. CONCLUSION

To conclude, we have studied the inertial-range anomalous scaling of a passive scalar quantity advected by the Gaussian velocity field, white in time and self-similar in space. The corresponding stochastic problem (1.1)–(1.3) can be reformulated as a field theoretic model (2.1), which allows one to identify the anomalous exponents with the critical dimensions of certain scalar and tensor composite operators built of the scalar gradients and to calculate them within the RG and OPE approach in the form of a regular perturbation expansion, similar to the well-known ε expansion in the RG theory of critical behavior.

Earlier, the anomalous exponents were presented to orders ε^2 [10–12,14] and ε^3 [15]; the main goal of the present paper has been the detailed explanation of the corresponding calculational techniques and derivation of the three-loop result, including the anisotropic sectors. Owing to the comparative universality of the RG and OPE formalism, these techniques can be applied to other models of dynamical critical phenomena and systems far from equilibrium: passive advection by the non-Gaussian velocities with finite correlation time, stochastic Navier-Stokes equation, and so on; see Refs. [13,21,22].

Another scope of the paper has been the discussion of the convergence properties of the ε expansion and the possibility of its extrapolation to finite values of ε. It was shown that the knowledge of three terms allows one to obtain reasonable predictions for finite $\varepsilon \sim 1$; even the plain ε expansion captures some subtle qualitative features of the anomalous exponents established in numerical experiments.

We believe that in the framework of the renormalization group and operator product expansion, the concept of dangerous composite operators and the ε expansion will become the necessary elements of the appearing theory of the anomalous scaling in fully developed turbulence.

APPENDIX: COEFFICIENTS A_i FOR THE THREE-LOOP DIAGRAMS

Below we give the pole parts of the coefficients A_i from Eq. (4.20) for all normal (not factorizable) three-loop dia-

grams. We use the following notation:

$$A_i = u^3 (\mu/m)^{3\varepsilon} \{ A_i^{(3)} \varepsilon^{-3} + A_i^{(2)} \varepsilon^{-2} + A_i^{(1)} \varepsilon^{-1} \},$$

$$A_i^{(3)} = (d-1) a_i(d) / 432 d^2 (d+2)^2.$$

Coefficients $A_i^{(1,2)}$ are given in Tables I and II for $d=2$ and $d=3$, respectively; coefficients $a_i(d)$ are given in Table III for general d.

---

[1] U. Frisch, *Turbulence: The Legacy of A. N. Kolmogorov* (Cambridge University Press, Cambridge, 1995).

[2] K.R. Sreenivasan and R.A. Antonia, Annu. Rev. Fluid Mech. **29**, 435 (1997).

[3] G. Falkovich, K. Gawȩdzki, and M. Vergassola, Rev. Mod. Phys. (to be published); e-print cond-mat/0105199.

[4] R.H. Kraichnan, Phys. Fluids **11**, 945 (1968); Phys. Rev. Lett. **72**, 1016 (1994); **78**, 4922 (1997).

[5] K. Gawȩdzki and A. Kupiainen, Phys. Rev. Lett. **75**, 3834 (1995); D. Bernard, K. Gawȩdzki, and A. Kupiainen, Phys. Rev. E **54**, 2564 (1996).

[6] M. Chertkov, G. Falkovich, I. Kolokolov, and V. Lebedev, Phys. Rev. E **52**, 4924 (1995); M. Chertkov and G. Falkovich, Phys. Rev. Lett. **76**, 2706 (1996).

[7] A. Pumir, Europhys. Lett. **34**, 25 (1996); **37**, 529 (1997); Phys. Rev. E **57**, 2914 (1998).

[8] B.I. Shraiman and E.D. Siggia, Phys. Rev. Lett. **77**, 2463 (1996); A. Pumir, B.I. Shraiman, and E.D. Siggia, Phys. Rev. E **55**, R1263 (1997).

[9] B. Duplantier and A. Ludwig, Phys. Rev. Lett. **66**, 247 (1991); G.L. Eyink, Phys. Lett. A **172**, 355 (1993); Phys. Rev. E **54**, 1497 (1996).

[10] L.Ts. Adzhemyan, N.V. Antonov, and A.N. Vasil'ev, Phys. Rev. E **58**, 1823 (1998).

[11] L.Ts. Adzhemyan and N.V. Antonov, Phys. Rev. E **58**, 7381 (1998).

[12] L.Ts. Adzhemyan, N.V. Antonov, and A.N. Vasil'ev, Theor. Math. Phys. **120**, 1074 (1999).

[13] N.V. Antonov, Phys. Rev. E **60**, 6691 (1999), Physica D **144**, 370 (2000).

[14] N.V. Antonov and J. Honkonen, Phys. Rev. E **63**, 036302 (2001).

[15] L.Ts. Adzhemyan, N.V. Antonov, V.A. Barinov, Yu.S. Kabrits, and A.N. Vasil'ev, Phys. Rev. E **63**, 025303(R) (2001); **64**, 019901(E) (2001).

[16] I. Arad, V. L'vov, E. Podivilov, and I. Procaccia, Phys. Rev. E **62**, 4904 (2000).

[17] K.J. Wiese, J. Stat. Phys. **101**, 843 (2000).

[18] N.V. Antonov, A. Lanotte, and A. Mazzino, Phys. Rev. E **61**, 6586 (2000).

[19] L. Ts. Adzhemyan, N. V. Antonov, A. Mazzino, P. Muratore-Ginanneschi, and A. V. Runov, Europhys. Lett. **55**, 801 (2001).

[20] L. Ts. Adzhemyan, N. V. Antonov, and A. V. Runov, Phys. Rev. E **64**, 046310 (2001).

[21] L.Ts. Adzhemyan, N.V. Antonov, and A.N. Vasil'ev, Usp. Fiz. Nauk **166**, 1257 (1996) [Phys. Usp. **39**, 1193 (1996)].

[22] L. Ts. Adzhemyan, N. V. Antonov, and A. N. Vasiliev, *The Field Theoretic Renormalization Group in Fully Developed Turbulence* (Gordon & Breach, London, 1999).

[23] U. Frisch, A. Mazzino, and M. Vergassola, Phys. Rev. Lett. **80**, 5532 (1998); Phys. Chem. Earth B **24**, 945 (1999).

[24] U. Frisch, A. Mazzino, A. Noullez, and M. Vergassola, Phys. Fluids **11**, 2178 (1999).

[25] A. Mazzino and P. Muratore-Ginanneschi, Phys. Rev. E **63**, 015302(R) (2001).

[26] A. N. Vasil'ev, *Functional Methods in Quantum Field Theory and Statistics* (Leningrad University Press, Leningrad, 1976) (in Russian; English translation: Gordon & Breach, London, 1998).

[27] A. P. Prudnikov, Y. A. Brychkov, and O. I. Marichev, *Integrals and Series* (Gordon & Breach, New York, 1986), Vols. 1 and 2.

[28] R.H. Kraichnan, J. Fluid Mech. **64**, 737 (1974).

[29] U. Frisch, J.D. Fournier, and H.A. Rose, J. Phys. A **11**, 187 (1978).

[30] A. V. Runov, St. Petersburg University Report No. SPbU-IP-99-08; e-print chao-dyn/9906026.

[31] A.L. Fairhall, O. Gat, V. L'vov, and I. Procaccia, Phys. Rev. E **53**, 3518 (1996).

[32] M. Chertkov, Phys. Rev. E **55**, 2722 (1997); E. Balkovsky and V. Lebedev, *ibid.* **58**, 5776 (1998).